CellPress

Matter

Review

Oxygen Redox Chemistry in Rechargeable Li-Ion and Na-Ion Batteries

Muhammad Mominur Rahman[1] and Feng Lin[1,*]

SUMMARY

Cationic redox-based oxide cathodes have formed the basis of alkali-ion batteries. The limited energy density provided by cationic redox can be overcome by triggering oxygen redox. Hence, oxygen redox has received extensive interest from the perspective of materials development and fundamental understanding. Although oxygen redox is widely studied, there is still much to understand. Consolidating various concepts of oxygen redox (static/dynamic) can inform a unified understanding. Moreover, materials with oxygen redox create significant challenges such as oxygen evolution, voltage hysteresis/fading, and chemical/structural transformations. A consensus is yet to be achieved on the interrelationship of these phenomena due to the chemical/structural complexities at different length and time scales. Given the great potential of these materials for next-generation batteries, a review of the recent understanding of oxygen redox is timely. In this review, the mechanistic understandings, and challenges and their mitigation with oxygen redox are summarized by integrating various schools of thought.

INTRODUCTION

A paradigm that oxide cathodes deliver reversible energy based on the redox activity of cations (transition metals) alone has been challenged by the fact that in many oxide electrodes, anions also take part in redox reactions. Li-rich layered materials and Li-excess disordered rocksalt (DRX) materials deliver excess capacity than the calculated capacity from the redox activity of the transition metals alone.[1] Today, it has been widely accepted that the excess capacity can be attributed to the redox activity of oxygen ions in addition to the transition metal ions.[2] The cumulative cationic and anionic redox has enabled the achievement of enhanced capacity and energy density. Hence, the development of materials combining anionic and cationic redox activities has become a focal point of research in Li/Na-ion batteries.[3,4]

Layered $LiCoO_2$ is one of the first commercial cathodes for Li-ion batteries and has enabled the widespread application of Li-ion batteries in many consumer electronics.[5] Further development of these cathode materials involved the partial substitution of Co by Ni and Mn (widely known as NMC materials).[6] NMC materials with high Ni content are desirable because of the high discharge capacity.[7,8] Due to the geopolitical issues with Co mining, a recent incentive is to reduce or completely eliminate Co from cathode materials.[9,10] Li-rich layered materials have attracted particular attention as an alternative to Co-based conventional NMC cathodes because they can provide larger than the theoretical capacity based on the cationic redox.[11–13] Initially, it was thought that the irreversible oxygen extraction and structural transformations account for the large irreversible capacity.[11,14] Later on,

Progress and Potential

Oxygen redox plays a critical role in breaking the energy density barrier of oxide cathodes for alkali-ion batteries. The development of advanced cathodes may take advantage of controllable oxygen redox along with conventional cationic redox. However, such development will require a clear understanding of oxygen redox chemistry. With the utilization of complementary multiscale synchrotron characterizations, the understanding of oxygen redox has developed over time. However, oxygen redox can polarize the opinion of experts as the static nature of oxidized oxygen, molecular oxygen, and peroxide formation has been reported. Meanwhile, prominent challenges such as voltage hysteresis and fading have been attributed to transition metal migration, oxygen evolution, and slow oxygen redox kinetics. However, a consensus is yet to be achieved. This review focuses on bridging many mechanisms and issues with oxygen redox so that a convenient understanding can be achieved by the reader.

through various studies, the reversible nature of the lattice oxygen redox was investigated.[15–18] Formulation of Li-excess DRX materials has further thrust oxygen redox chemistry into the limelight.[19,20] These materials deliver high capacity owing to the combined anionic and cationic redox activities without the need for a well-defined structural ordering for Li percolation. Hence, many transition metals can be utilized for designing these materials, which also vastly expands the compositional space for developing cathode materials with cheap transition metals.[21,22]

Charging conventional layered oxides to a very high voltage (close to 5.0 V) has been reported to lead to lattice oxygen redox.[23,24] In a conventional layered material, electron holes can be localized in the O 2p molecular orbital, leading to the oxidation of oxygen anions at high states of charge.[25] Meanwhile, Ceder and coworkers showed that the Li-O-Li configurations are important for forming oxygen 2p orbitals prone to oxygen redox, which can be achieved in Li-rich stoichiometry or through structural disordering.[15] While some of the models explain the oxygen redox to be static in nature,[15] other models predict them to be dynamic.[26] For example, some studies claim structural reorganization takes place on the oxidized oxygen to form peroxo-like species[27] as well as transition metal migration that can modify the crystal and electronic structures of cathode materials.[28] Voltage fadings are significant issues in these materials, which are claimed to be caused by irreversible transition metal migration and could be accelerated by oxygen redox, although the exact mechanism remains debatable.[28–31] It is clear that there are various mechanisms being put forward toward understanding oxygen redox and related stability issues. In this review, we compile a consolidated report on the mechanism of oxygen redox and related issues with irreversibility of oxygen redox. A mechanistic explanation is first presented by providing accounts of both static and dynamic nature of oxygen redox. This is followed by a discussion of Li and Na cathode materials in which oxygen redox was confirmed through spectroscopic and computational studies. Challenges with oxygen redox and mitigation strategies are explained thereafter.

MECHANISMS OF OXYGEN REDOX

Oxygen redox in oxide electrodes mainly refers to the evolution of oxidation states of lattice oxygen that leads to reversible capacity during cycling.[32] The voltage of the conventional layered oxide cathodes is limited by the top of the O 2p bands. In layered oxides, removal of alkali ion during charging strengthens the transition metal (TM)3d-O2p hybridization. However, at deeper delithiation level (e.g., $x > 0.55$ in $Li_{1-x}CoO_2$), the holes created due to the removal of electron gets trapped in the O 2p orbitals, followed by oxygen evolution.[25] This type of oxygen activity is irreversible and does not lead to usable charge/discharge capacity on long-term cycling. However, recent works show that the oxygen redox at high states of charge in conventional layered oxides is not entirely irreversible and can lead to usable capacity.[23,24,33] Reversible oxygen redox in conventional layered oxides is discussed in more detail later.

Reversible oxygen redox is widely studied in Li-rich materials. The work of Ceder and coworkers explored the structural and chemical characteristics of triggering oxygen redox in Li-rich layered oxide cathodes.[15] They performed density functional theory (DFT)-based calculations utilizing the Heyd-Scuseria-Ernzerhof (HSE06) hybrid functional on a series of Li-rich layered and disordered rocksalt materials (Figures 1A–1C). Their calculation showed an increase in partial density of states (pDOS) from the oxygen states between 0 and −2.5 V (Figure 1B). The charge density plot around oxygen confirmed that within the shaded region of the pDOS plot, the charge

[1]Department of Chemistry, Virginia Tech, Blacksburg, VA 24061, USA

*Correspondence: fenglin@vt.edu

https://doi.org/10.1016/j.matt.2020.12.004

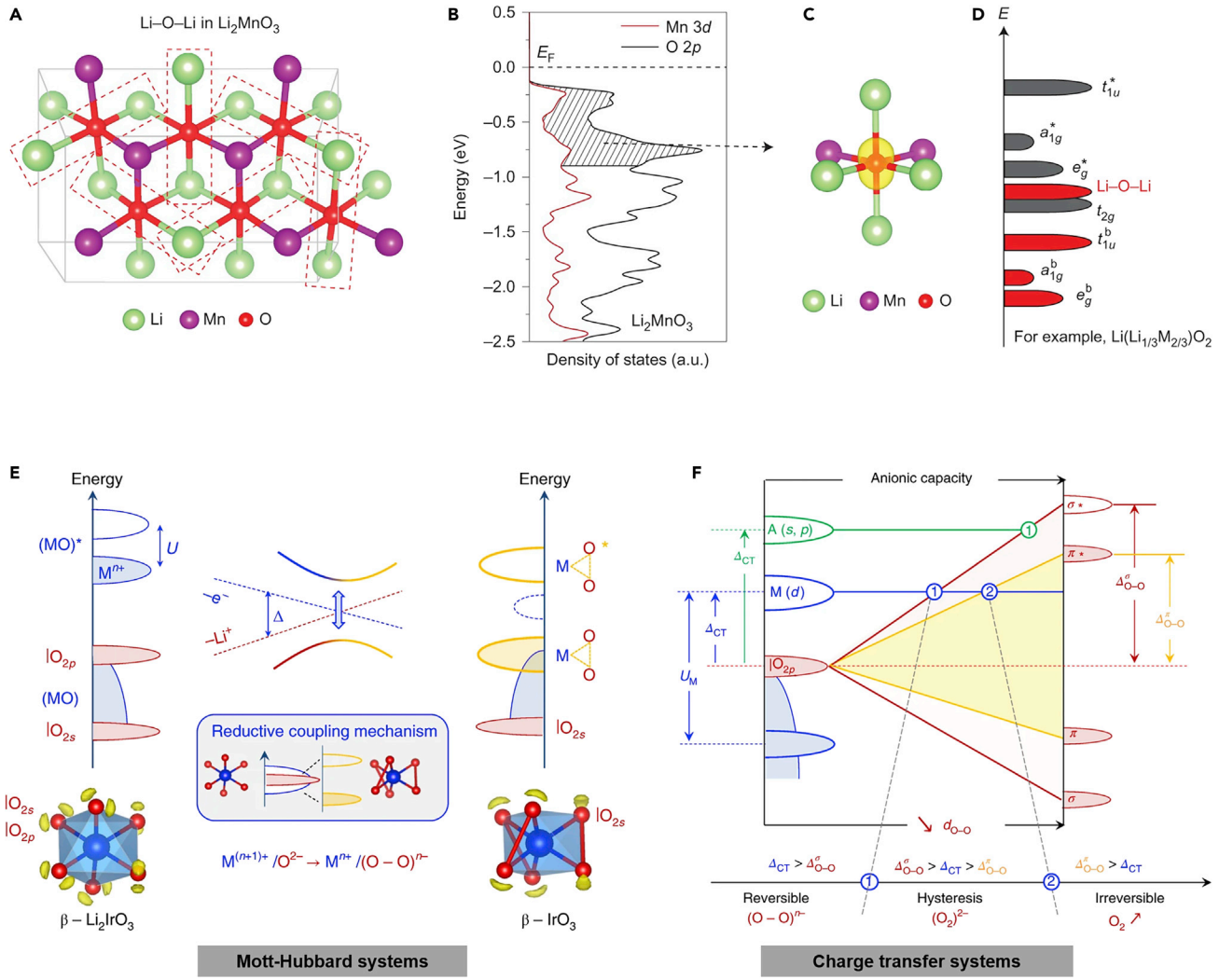

Figure 1. Mechanism of Oxygen Redox in Alkali-Rich Oxide-Based Cathodes for Alkali-Ion Batteries

(A) Li-O-Li configurations in Li_2MnO_3.

(B) A plot showing the pDOS of O 2p orbitals and the Mn 3d orbitals in Li_2MnO_3. A larger pDOS arises from the O 2p orbitals in the shaded region of the plot.

(C) Isosurface of the charge density around the O 2p orbital in the shaded region of the pDOS plot.

(D) Schematic representation of the electronic band structure of Li_2MnO_3. Adapted from Seo et al.[15] Unhybridized O 2p orbitals arise in the Li-O-Li configuration, which are higher in energy than the bonding molecular orbitals but lower in energy than the antibonding molecular orbitals.

(E) Electronic structure evolution of a Mott-Hubbard system upon alkali-ion removal. Schematic band structure of a Mott-Hubbard system (on the left). The electrostatic stabilization of the (M–O)* states upon electron removal is shown by the blue dashed line. The electrostatic destabilization of the O 2p lone pair electrons upon Li^+ removal is shown by the red dashed line. Reductive coupling mechanism through a ligand (oxygen ions) to metal charge transfer is shown in the inset. The schematic band structure as a result of the reductive coupling mechanism is shown on the right.

(F) Electronic structure evolution in charge transfer systems upon alkali-ion removal. The O 2p orbital splits into σ, π, σ*, and π* states with increasing anionic capacity, as highlighted by the red and yellow triangles. Adapted from Ben Yahia et al.[26]

density resembled an isolated O 2p orbital lying in the direction of the Li-O-Li axis (Figure 1C). The enhanced charge density around the oxygen ion because of the Li-O-Li configuration near the Fermi level indicated that these electrons from oxygen are prone to participate in redox reactions during electrochemical cycling. This can be further visualized by the schematic of the electronic band structure of the Li-rich materials in Figure 1D. The O 2p orbital in the Li-O-Li configuration cannot hybridize with the Li 2s orbital because of the large energy difference. Hence, these O 2p

orbitals remain unhybridized. The energy of these unhybridized orbitals is higher than that of the bonding orbitals (e.g., t^{b}_{1u}) but lower than that of the antibonding metal states (e.g., e^{*}_{g}). Whether these unhybridized O 2p orbitals or the transition metal cation will oxidize first depends on the energy level of the d states of the transition metal ions. If a transition metal (e.g., Mn 3d)[15] has a higher energy level of the 3d orbital compared with another transition metal (e.g., Ni 3d),[15] the corresponding e_g* state will also be higher in energy. This will cause a lesser overlap between the e^{*}_{g} state and the unhybridized O 2p orbital, resulting in better utilization of the transition metal redox. Meanwhile, in certain cases, the oxidized oxygen has been reported to form peroxo-like species.[27] According to the authors, the peroxo-like bond will be formed when the oxygen is bonded to non-transition metals, such as Sb and Sn. The relatively free rotation of the Li-O-Li configuration allows for the formation of a weak sigma bond between two oxygens. Formation of peroxo-like species is difficult for transition metals with partially filled d orbitals because of the strong directionality of the d orbitals (e.g., Mn, Ni, Co). Meanwhile, Doublet and coworkers proposed the charge-transfer gap of Li-rich oxides as an indicator of oxygen redox and its reversibility.[26] The authors classified the oxide cathodes into two categories: Mott-Hubbard system (partially filled metal bands) and charge-transfer systems (empty metal bands).[34] In the Mott-Hubbard-type Li-rich oxides, the partially filled metal bands will empty first, resulting in the destabilization of the O 2p lone pairs and the stabilization of the (M–O)* states (Figure 1E). At the delithiation point beyond the degeneracy level of these two bands, structural distortion must take place to form M–(O–O) species to stabilize the oxidized oxygen. Such coupling will take place with the concomitant reduction of the transition metals, hence the name "reductive coupling mechanism." In contrast, in the charge-transfer type Li-rich metal oxides, the anionic band will empty first on delithiation and the oxidized oxygen must recombine to satisfy the octet rule (Figure 1F). This recombination will lead to the splitting of the anionic band (marked by $|O_{2p}$ in Figure 1F) to the formation of π, π^*, σ, and σ^* bands. The separation between the filled anionic band and empty metallic band (M(d)), Δ_{CT}, and Δ^{π}_{O-O} are taken as pertinent parameters to predict oxygen redox reversibility. As long as Δ_{CT} is bigger than Δ^{π}_{O-O}, the oxygen redox will be reversible and a reductive coupling mechanism can take place. However, when Δ_{CT} is smaller than Δ^{π}_{O-O} (with an increase in anionic capacity), oxygen evolution takes place through a "reductive elimination mechanism." Doublet and coworkers argued that the coupling between oxidized oxygens (formation of peroxo-like species) and/or transition metal migration are crucial factors in stabilizing oxygen redox irrespective of the partially filled or empty metal d bands. Further computational work by them showed that formation of peroxo-like species is possible in $Li_{2-x}RuO_3$ and that the formation of this species is not linked to the presence of elements such as Sn, Ti, and Mn,[35] much in contrast to other studies that emphasized the importance of non-transition metals for the formation of peroxo-like species.[15] A study by Zhou and coworkers claimed to visualize peroxo-like species in $Li_{1.2}Ni_{0.2}Mn_{0.6}O_2$ through X-ray diffraction (XRD) and Raman spectroscopy.[36] Peroxo-like species are also reported in $Li_2Ru_{1-y}Sn_yO_3$ based on X-ray photoelectron spectroscopy (XPS) study.[37] However, the rationalization of oxygen redox based on XPS was challenged recently by the work of Piper and coworkers. They mention that the O1s peak in the region of 530–531 eV observed at high states of charge can be rationalized in terms of transition metal reduction and electrolyte decomposition rather than lattice oxygen oxidation.[38] Recent studies have predicted that the oxygen redox cannot be explained by a rigid O^{2-}/O^{-} redox couple and must take into account structural and electronic changes upon oxygen redox.[28,39] In Li/Mn-rich materials (abbreviated as LMR), oxygen oxidation is accompanied by transition metal migration to the Li site.[28,30] Such migration changes the

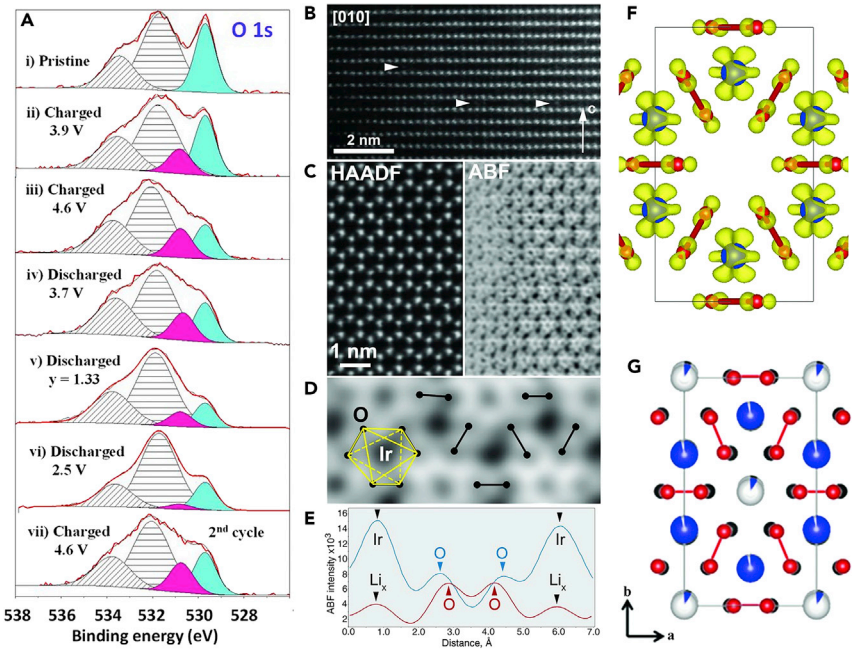

Figure 2. Studying the Nature of the Oxidized Oxygen in Li_2IrO_3 Cathodes during Electrochemical Cycling

(A) XPS spectra at different states of charge to show the evolution of the chemical nature of the oxygen ion.

(B) [010] HAADF-STEM images of $Li_{0.5}IrO_3$ (charged state). The white arrows mark antisite point defects.

(C) [001] HAADF-STEM image (left) and ABF-STEM image (right) of $Li_{0.5}IrO_3$.

(D) Zoomed-in view of the ABF-STEM image in C. The O–O pairs with shortened distance are shown as black dumbbells. The lengthened projected O–O separations are left blank. The twisting of the IrO_6 octahedra (shown in yellow) gives rise to the O–O pairs.

(E) ABF intensity profile showing the long (blue) and short (red) O–O pair distances.

(F) O1 stacking sequence of the charged $Li_{0.5}IrO_3$ along the [001] projection, calculated through DFT. Oxygen and Ir atoms are represented in red and blue, respectively. The Fukui orbitals are shown in yellow.

(G) Structure of the charged material deciphered from the neutron powder diffraction. The pristine structure is shown in black, on which the charged structure is superimposed. Adapted from McCalla et al.[27]

electrostatic environment surrounding the oxidized oxygen and shifts the O 2p states to higher energy compared with the TM-O hybridized states. This reshuffling reduces the redox potential of the bulk oxygen redox couple during electrochemical cycling, which according to the authors cannot be explained by a rigid O^{2-}/O^{-} redox model. It is evident that the true chemical nature of the oxidized oxygen is still under debate, and the understanding of oxygen redox is likely to evolve over time.

Nevertheless, the visualization of peroxo-like species in Li cathodes with oxygen redox was reported by McCalla et al. based on their work in Li_2IrO_3.[27] The oxidation of O^{2-} was studied through XPS spectra at different states of charge (red peak in Figure 2A), which took place concomitant to Ir^{4+} oxidation. The authors argued the oxidized oxygen formed peroxo-like species. The formation of this peroxo species takes place through a local distortion of the oxygen lattice. Such distortion was probed by high-angle annular dark-field scanning transmission electron microscopy (HAADF-STEM), annular bright-field scanning transmission electron microscopy (ABF-STEM) (Figures 2B–2E), DFT calculations (Figure 2F), and structural analysis through neutron powder diffraction

(Figure 2G). The authors argued that since the material assumed an O1 type structure at the end of charge, the visualization of the oxygen lattice was possible in the c direction without the interference from Ir or Li. Their analysis showed that the symmetry of the IrO_6 octahedron decreased from sixfold to threefold because of the formation of the shortened (black dumbbells in Figure 2D) and lengthened O–O separations (left blank). Such shortening of the O–O distance was attributed to peroxo-like species through DFT calculations (red dumbbells in Figure 2F) and neutron powder diffraction refinement (Figure 2G). The Fukui function (yellow surface in Figure 2F) displays overlapping lobes in the direction of O–O pairs, which the authors attributed to partially empty antibonding σ* orbitals from peroxo-like species.

Recently, Bruce and coworkers proposed molecular O_2 formation as one of the models of lattice oxygen redox.[40,41] In a material where alkali ions in the transition metal layer are in honeycomb ordering with the transition metals, all oxygen atoms are coordinated with two transition metals. Upon oxidizing lattice oxygen, alkali ions in the transition metal layer can move to the alkali layer and transition metal migration can break the degeneracy in energy, forming oxidized oxygen coordinated with three to no transition metals. The oxidized oxygen coordinated with no transition metal can stabilize through dimerization with oxygen coordinated with one transition metal. Upon discharging, the O–O bond is cleaved through the reduction of the unoccupied states in O_2.[41] Molecular oxygen formation on the bulk of the material has been supported by resonant inelastic X-ray scattering (RIXS), which shows energy-loss peaks corresponding to O–O bond vibrations similar to molecular O_2.[41] The proposed model of molecular oxygen formation has provided an alternative explanation to the oxygen redox chemistry. On the other hand, some studies mention subtle nuances in the RIXS maps of molecular O_2 and oxidized lattice oxygen in battery materials.[42] It is clear that the nature of lattice oxygen redox still remains elusive, and further investigations are required.

In summary, oxygen redox in battery cathodes is closely related to the energy of the TM (*n*)d bands and the O 2p bands.[25] At deep delithiation/desodiation level, electron holes can be localized on the O 2p bands, making them redox active. Li-rich stoichiometry has enabled tuning of the oxygen redox chemistry in battery cathodes. The work of Ceder and coworkers has established Li-O-Li configurations as a critical structural unit for triggering oxygen redox in Li-rich layered and DRX materials.[15] Unhybridized O 2p orbitals are created along the Li-O-Li configurations which are close to Fermi level, making them potentially redox active. Even though there is general consensus about triggering oxygen redox in Li-rich cathode materials, the account of the consequence of oxygen redox varies significantly. Some studies point out structural reorganization to stabilize oxygen redox with coupling between the oxidized oxygen, irrespective of the material composition.[26,35] Other studies indicate the type of the transition metal element to which the oxidized oxygen is bonded is critical for peroxo-like dimer formation.[15] Peroxo-like species, molecular O_2 formation, and localized electron holes in O 2p orbitals have been reported in the literature.[27,41,43] Indeed, it is critical to truly reveal the chemical nature of oxidized oxygen in the battery cathode materials. With the advancement of characterization techniques for probing oxygen redox, attainment of such understanding might become possible, as discussed in detail later.

CHARACTERIZATION OF OXYGEN REDOX REACTIONS

Many studies probe oxygen redox through XPS.[44–46] However, XPS is a surface-sensitive technique that can give information about the redox evolution only on the surface region of particles and electrodes. Hence, XPS cannot provide conclusive evidence as

to whether such redox process is a bulk phenomenon or only limited to the surface. It is notable that by utilizing high-energy synchrotron X-rays, the probing depth of XPS can be enhanced to 40 nm at 10.0-keV incident energy.[45] Another challenge facing surface-sensitive XPS is associated with the formation of complex cathode-electrolyte interphase that may interfere with the XPS signal from the lattice oxygen. Fitting of the O 1s XPS spectrum shows a feature in the range of 530–531 eV, which has been attributed to the lattice oxygen redox process. However, Piper and coworkers attributed the peak within this range to transition metal reduction and electrolyte decomposition,[38] which puts into question the reliability of fitting the O1s XPS spectrum to show lattice oxygen redox. O K-edge X-ray absorption spectroscopy (XAS) spectra derived from soft XAS has also been utilized to provide evidence of oxygen redox. However, caution should be taken on interpreting the O K-edge spectrum because it predominantly gives information about the evolution of TM3d-O 2p hybridization on electrochemical cycling rather than probing the localized hole states on O 2p orbitals.[47,48] Nevertheless, since soft XAS directly probes the TM3d-O 2p hybridization, indirect information on oxygen redox reactions can be obtained in some particular cases. On the high-voltage plateau region of materials showing oxygen redox, minimum oxidation of transition metals is reported in many cases.[49] The increase in pre-edge peak area of O K-edge at the high-voltage plateau region can be reasonably attributed to the oxidation of oxygen anions in those cases.[49] Perhaps more direct and convincing spectroscopic evidence of oxygen redox is obtained through RIXS. RIXS has a probing depth similar to that of fluorescence yield of soft XAS and can provide information up to about 100-nm depth of a particle.[50] The reliability of RIXS over XAS for probing oxygen redox reactions stems from the ability to resolve the emission energy of fluorescence photons that is not possible in conventional XAS. Such resolution has enabled discernment of the fingerprint feature of oxidized oxygen, which is typically buried in XAS. An RIXS map (Figure 3A) will consist of features predominantly at around 525-eV emission energy. The excitation energies of 529 eV and 532 eV corresponding to the same emission energy of 525 eV is assigned to TM3d-O 2p hybridization while the excitation energy at >534 eV can be assigned to O 2p bands of O^{2-} hybridized with TM4s/4p states. Interestingly, for the charged $Na_{2/3}Mg_{1/3}Mn_{2/3}O_2$ cathode in Figure 3A, an additional feature is observed at 523.7-eV emission energy for corresponding 531-eV excitation energy. Such experimental observation, along with theoretical calculation based on the OCEAN package, of Li_2O_2 has shown that the feature is generated from the O 2p-O 2p intraband excitation.[51] This interaction requires unoccupied O 2p orbitals, which are absent in O^{2-} and is a sign of oxygen redox. However, further studies of Li_2O_2, O_2, and CO_2 systems indicate that this RIXS feature interpretation is beyond a simple molecular model with unoccupied O 2p states because the highly covalent CO_2 system does not display such a feature.[42] At this time, theoretical calculation of the oxygen redox signature in RIXS maps remains a major challenge but holds the promise to reveal the fundamental mechanism of oxygen redox. For example, resolving the energy of the emission photons reveals critical information on the nature of the lattice oxygen redox reactions, including subtlety in RIXS signals of Li_2O_2, O_2, and materials showing lattice oxygen redox.[42] This warrants further investigation to reveal the true nature of the lattice oxygen redox. Nonetheless, integrating the red boxed region showing the lattice oxygen redox (Figure 3A) yields a spectrum (red spectrum in Figure 3B) that has clearly different spectral features than when the spectrum is obtained (blue spectrum in Figure 3B) by integrating the blue boxed region (containing the intensity map of pre-edge and O K-edge in Figure 3A). However, integration of the RIXS intensity map on a much wider excitation and emission energy range (green box in Figure 3A) would yield a spectrum wherein this distinction of the oxygen redox signal is completely absent (green spectrum in Figure 3B). The features for this integrated spectrum (TM3d-O 2p hybridization and O 2p bands of O^{2-}) match with the energy for the

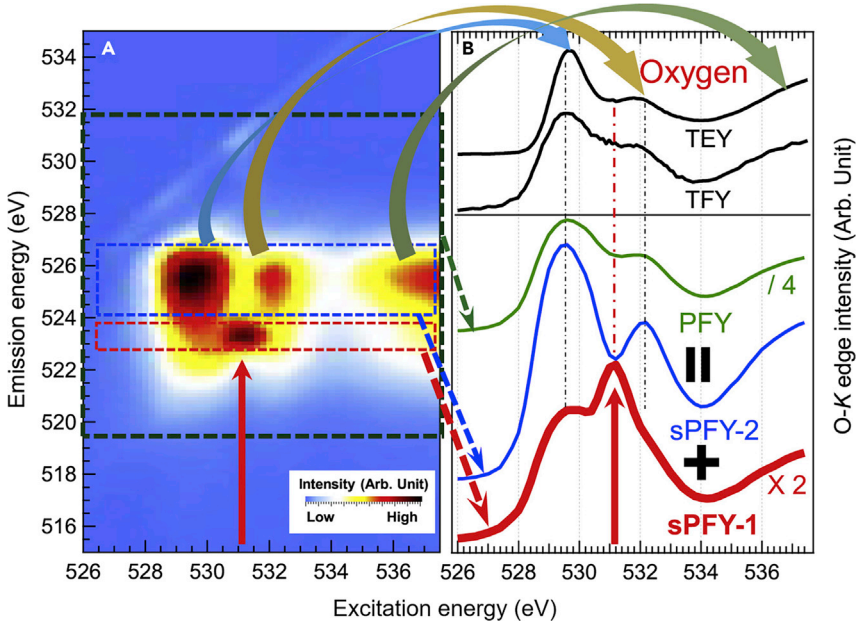

Figure 3. Oxygen Redox Process in Oxide Cathodes Probed by Resonant Inelastic X-ray Scattering

(A) O K-edge mapping of resonant inelastic X-ray scattering (RIXS) of charged $Na_{2/3}Mg_{1/3}Mn_{2/3}O_2$ cathode.

(B) The super-partial fluorescence yield (sPFY) spectra (colored blue and red) are obtained by integrating the signal on the boxed region of same color on the RIXS map in (A). Integrating at a wider region (green box in A) gives the spectrum colored green. The conventional partial fluorescence yield (PFY; green spectrum), total fluorescence yield (TFY; in black), and total electron yield (TEY; in black) are also shown for comparison. Adapted from Dai et al.[50] PFY is generated when the fluorescence photons are discriminated based on their energy. TEY is generated from both auger electron and photoelectron.

conventional XAS and show why the conventional XAS cannot decipher the true lattice oxygen redox. Furthermore, the bulk sensitivity of RIXS can be enhanced if the surface signal is differentiated from the bulk.[47] Spatially resolved scanning transmission X-ray microscopy has shown a feature at 531-eV excitation energy on the bulk of charged Li/Mn-rich materials.[28] The RIXS map shows a feature at the same excitation energy for the oxidized lattice oxygen (Figure 3), which proves that the oxygen redox is a bulk phenomenon.

Pair distribution function (PDF) analysis can probe the local structural rearrangement associated with oxygen redox reactions.[52] By utilizing both Bragg diffraction and diffuse scattering signal, PDF can provide local structural changes and short-range ordering.[53] Neutron PDF holds an advantage over X-ray PDF because it is sensitive toward lighter atoms such as oxygen. Hence, most local structural changes associated with the lattice oxygen framework can be probed by neutron PDF analysis. Through utilizing such a technique, short O–O pair formation similar to peroxo-like dimer has been reported in charged P3-type $Na_{0.6}[Li_{0.2}Mn_{0.8}]O_2$ samples, similar to Li_2IrO_3.[27,52]

MATERIALS SHOWING OXYGEN REDOX

Oxygen Redox in Alkali-Rich Layered Transition Metal Oxides

Several research groups have extensively explored the synthesis, structural, and electrochemical characterization of various Li-rich layered oxide materials ($Li_{1+x}TM_{1-x}O_2$, where TM is a 3d transition metal or a combination of different

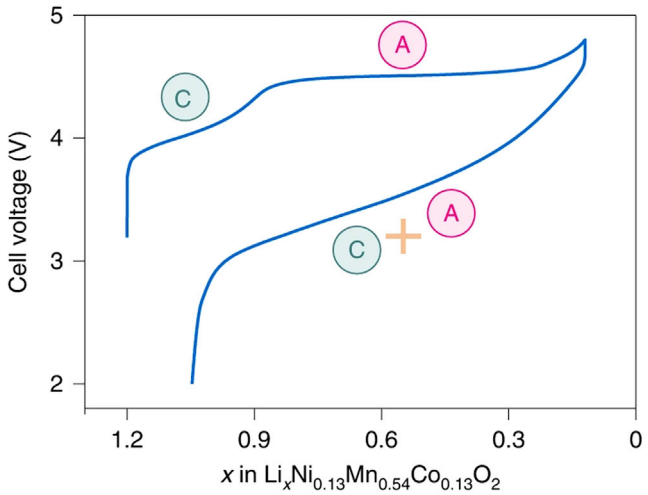

Figure 4. Voltage Hysteresis in Li-Rich Layered Materials

First-cycle charge-discharge curves of Li-rich NMC material. The regions marked by C and A denote cationic and anionic redox reactions, respectively. Voltage hysteresis is displayed as the charge and discharge curves do not trace the same path. Adapted from Assat et al.[123]

transition metals).[11,12,54–61] A large characteristic voltage plateau and irreversible capacity were observed in these materials at the first cycle (Figure 4). Initial theories of the excess capacity included Mn oxidation to +5 state, irreversible extraction of oxygen on the high-voltage plateau region,[11] and extraction of Li_2O (lithia) from the Li_2MnO_3 domain of the composite structured Li-rich cathodes.[58] However, a reversible participation of lattice oxygen was not mentioned. The contribution of oxygen to charge compensation without oxygen loss on Li-rich layered $Li[Li_{0.15}Ni_{0.275-x}Mg_xMn_{0.575}]O_2$ was speculated by Amine and coworkers back in 2003 based on their XAS study.[59] An increase in pre-edge peak area was taken as a sign of oxygen redox, and it is now well known that the pre-edge feature is mostly dominated by TM3d–O 2p hybridization and not the localized hole states on the O 2p orbitals, as discussed in the Introduction.

The reversible/irreversible nature of the surface-to-bulk oxygen redox activity in Li-rich layered materials was investigated by the works of Delmas and coworkers in 2013[62,63] and later by Bruce and coworkers.[16,64] Delmas' group argued that the observed initial discharge capacity of more than 270 mAh/g in $Li_{1.20}Mn_{0.54}Co_{0.13}Ni_{0.13}O_2$ can only be explained if both irreversible oxygen redox in the form of oxygen loss from the surface of the particle and reversible oxygen redox in the bulk of the particle are taken into account.[62] Oxygen redox in $Li_{1.20}Mn_{0.54}Co_{0.13}Ni_{0.13}O_2$ was further probed and quantified by Bruce and coworkers through *operando* differential electrochemical mass spectrometry (DEMS), Raman spectroscopy, XAS, and RIXS.[16] To estimate the irreversible nature of the oxygen redox, the authors labeled the oxygen in the material with ^{18}O isotope. Time-of-flight secondary ion mass spectrometry indicated that a total of 15% ^{18}O enrichment in the lattice oxygen was obtained. Hence, the evolved gases from the irreversible lattice oxygen redox activity during electrochemical cycling must have a certain ratio of $^{16}O/^{18}O$. Their DEMS study revealed that on the 4.5-V plateau region, even though there was no molecular O_2 evolution, a detectable amount of CO_2 was measured (Figure 5C). The CO_2 evolution was also observed at very high states of charge (close to 4.8 V). The total $^{16}O/^{18}O$ ratio in the evolved CO_2 was close to that of the expected ratio if all the evolved CO_2 was accounted for only by the reaction of the lattice oxygen with the

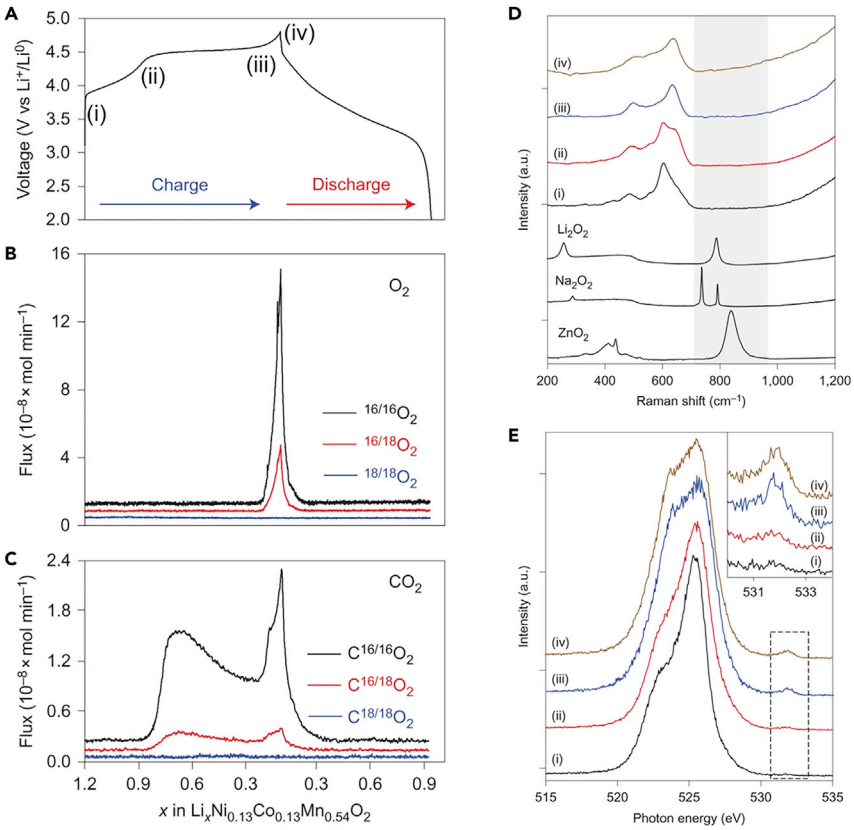

Figure 5. Probing the Reversible and Irreversible Oxygen Redox in $Li_{1.20}Mn_{0.54}Co_{0.13}Ni_{0.13}O_2$

(A) First-cycle charge and discharge curves of $Li_{1.20}Mn_{0.54}Co_{0.13}Ni_{0.13}O_2$. The labels (i) to (iv) indicate the state of charge in which Raman and RIXS spectra were taken in (D) and (E).

(B and C) Quantifying the evolution of (B) gaseous O_2, and (C) CO_2 during cycling, measured through *operando* differential electrochemical mass spectrometry (DEMS).

(D and E) Probing the chemical nature of the oxidized oxygen through (D) Raman spectroscopy and (E) RIXS. Gas evolution through DEMS probes irreversible oxygen redox, whereas RIXS probes reversible oxygen redox. Adapted from Luo et al.[16]

electrolyte (expected: 20%; experimental: 13%). Even when taking the discrepancy between the expected and experimental percentages into account, it is clear that most of the CO_2 evolution occurred from the contribution of the lattice oxygen. At high states of charge (close to 4.8 V), significant O_2 evolution occurred (Figure 5B) and the ratio of $^{16}O/^{18}O$ in O_2 was close to what was expected if the evolved oxygen came only from the contribution of the lattice oxygen (expected: 26%; experimental: 23%). Even though oxygen evolution could account for most of the capacity obtained at the sloping region beyond the 4.5-V plateau (Figure 5A), the irreversible oxygen redox reactions at the plateau region could only account for 9% of the total charge capacity obtained at that region. Hence, a significant portion of the charge capacity was obtained by a reversible oxygen redox, as DEMS can only measure irreversible oxygen evolution. A reversible oxygen redox is expected to create hole states in the O 2p orbitals but those hole states did not create O–O dimers (no peaks similar to peroxide are observed in Figure 5D), unlike Li-rich materials with 4d or 5d transition metals (see Mechanisms of Oxygen Redox for more details). Instead, the authors argued that the hole states were localized in nature as signified by the broadening of the RIXS spectrum and the formation of an elastic peak at around 532 eV (boxed region in Figure 5E). Hence, the analyses carried out by Bruce and

coworkers indicated that the oxygen redox is both reversible and irreversible in nature as opposed to the early model of only irreversible oxygen redox proposed to explain the enhanced capacity delivered by these materials.[11]

Li_2TMO_3 or $Li[Li_{1/3}TM_{2/3}]O_2$ (where TM is either 4d or 5d transition metals) studied in detail by Tarascon and coworkers also delivers excess capacity through oxygen redox.[27,37,65] In case the Li and TM in the transition metal layer are ordered, only one type of oxygen sublattice where all O should have one Li-O-Li configuration is expected.[26] It is argued that the peroxo-like O–O dimer in materials such as Li_2RuO_3 and $Li_2Ru_{1-y}Sn_yO_2$ forms through a "reductive coupling mechanism" (see Mechanisms of Oxygen Redox for more details).[26,35,37] Such structural reorganization stabilizes oxygen redox in these materials. Similar to Li-rich oxides with 3d transition metals, a large high-voltage plateau is observed, and oxygen redox plays a significant role in the charge-compensation mechanism.[27] Na-rich transition metal oxides with 4d and 5d transition metals and the general formula Na_2TMO_3 also show oxygen redox activity during electrochemical cycling.[66–69]

Similar to oxygen redox chemistry in Li-rich materials, the understanding of the crystal structure of these materials has also evolved over time. Li-rich materials are thought of either as a single-phase solid solution with trigonal structure where all the Li and transition metal ions are distributed in the transition metal layer with long-range ordering[13,70] or as a single-phase monoclinic structure throughout.[71] They are also viewed as a composite of Li_2MnO_3-$LiTMO_2$ with close structural compatibility, with Li and Mn in the Li_2MnO_3 domains having honeycomb-like ordering.[72–74] The actual crystal structure arrangement has sparked a long-standing debate in the research community. Here, we summarize the claims from both ends (single-phase or composite).

One of the first claims of the composite nature of the Li-rich materials was made by Thackeray and coworkers.[14,75] Experimental verifications of the composite nature of $Li_{1.2}Mn_{0.55}Ni_{0.15}Co_{0.10}O_2$ (commercially known as TODA HE5050) were provided through neutron diffraction and magnetic susceptibility studies.[72] Two models were chosen by the authors for neutron diffraction refinement: a single monoclinic phase throughout with a C2/m space group, and a composite of a monoclinic phase with a C2/m space group and a trigonal phase with an $R\bar{3}m$ space group. Reasonable fitting was obtained for both models. For example, a fitting model with the composite structure of a monoclinic phase with only Li and Mn and a trigonal phase with all three transition metals and Li is shown in Figure 6A. The Li- and Mn-containing phase had Li/Mn ordering, which explained the superstructure peaks in the pattern. Moreover, including a 3% Li/Ni site exchange increased the reliability of the fitting. To conclusively choose between the composite or single-phase models, the authors further performed a temperature-dependent magnetic susceptibility study (Figure 6B). From the magnetic susceptibility study, it can be seen that the field-cooling (FC) and the zero-field-cooling (ZFC) curves follow each other up to 100 K, which the authors attributed to the disordering of the transition metals in the trigonal phase (one component of the composite structure). At temperature lower than 100 K, the curves diverge from each other due to a magnetic ordering in the material, which the authors attributed to the Li/Mn ordering in the Li_2MnO_3 phase of the material (the other component of the composite structure). Even though some studies claim the composite nature of the Li-rich materials based on transmission electron microscopy,[73] such multiphase composite structure is highly debated. Dahn and coworkers argued that certain transition-metal-rich domains such as the Li_2MnO_3 are unlikely because the high-temperature synthesis should not allow the clustering of a particular transition metal from the entropic perspective.[13] The counterclaim against the composite nature of the Li-rich materials is now discussed.

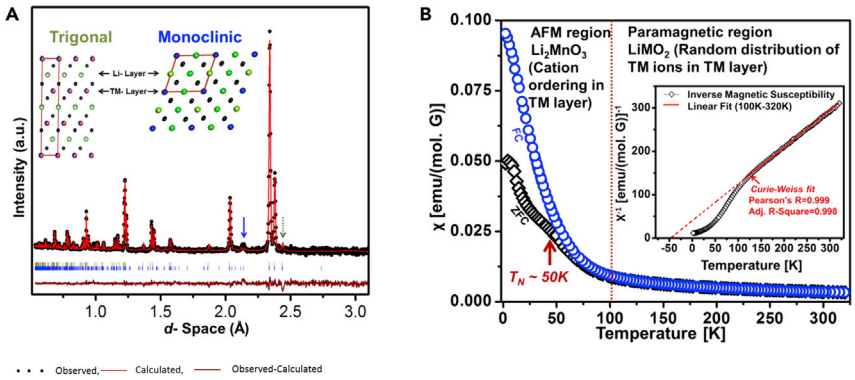

Figure 6. Experiments Illustrating the Composite Nature of the Li-Rich Layered Materials

(A) Refinement of the neutron diffraction pattern of $Li_{1.2}Mn_{0.55}Ni_{0.15}Co_{0.10}O_2$ (TODA HE5050) by considering a biphasic model (monoclinic and trigonal).

(B) Magnetic susceptibility study of $Li_{1.2}Mn_{0.55}Ni_{0.15}Co_{0.10}O_2$ to provide evidence between single-phase and composite structure. The divergence of the FC and ZFC curves at lower than 100 K was attributed to the ordering of Li/Mn in Li_2MnO_3 component of the composite material. The Curie-Weiss fit of the inverse magnetic susceptibility is shown in the inset. Adapted from Mohanty et al.[72]

It is necessary to provide visual representations of the phases at the single-particle level in addition to structural refinement analysis to prevent any structural ambiguity. High-resolution TEM (HRTEM) imaging can be one such way, but the small field of view of the HRTEM imaging cannot unanimously prove whether a material is a single phase or of composite nature. Shukla et al. provided a comprehensive TEM analysis on the nature of the phases present in $Li_{1.20}Mn_{0.54}Co_{0.13}Ni_{0.13}O_2$ by imaging the particles of this material at a much larger field of view (Figure 7).[71] The needle-like particles with small thickness enabled imaging of the whole primary particle with atomic resolution (Figures 7C and 7G). HAADF images showed that there was no sign of composite nature in the material. Instead, the crystal structure of the material consisted of three different variants of the monoclinic phases alternating between each other randomly (colored boxes in Figure 7A and colored rows in Figure 7B). The three variants of the monoclinic phases are defined by the projections along the [100], [110], and [$1\bar{1}0$] directions, as shown in Figures 7D–7F. Meanwhile, imaging at a much larger field of view did not show any presence of the composite nature of the material (Figures 7C and 7G). The authors made similar observations in commercial Li-rich TODA HE5050 material, in contrast to the study summarized earlier.[72] It must be mentioned that whether the structural ambiguity with the Li-rich materials was raised because of the different synthesis method and composition used by different groups or from the misinterpretation of the TEM data is not clearly understood. Shukla et al. provided one such example that because of the different stacking of more than one monoclinic variant in the thicker regions of the particle, those regions may assume hexagonal ordering when viewed from a certain direction. This may lead to the erroneous assignment of trigonal phases to these regions. More study is needed to clear up the confusion regarding the composite versus single-phase debate in the Li-rich materials. However, it seems that the oxygen redox chemistry takes place in these materials independent of the debate.

Oxygen Redox in Conventional Layered Transition Metal Oxides

The contribution of oxygen to the charge-compensation mechanism in conventional layered $LiTMO_2$ with no Li excess (e.g., $LiCoO_2$, $LiNi_{0.5}Co_{0.5}O_2$) was claimed in the early 2000s,[76–78] even before the general acceptance of significant reversible oxygen redox in Li-rich materials. However, these studies were based on observations

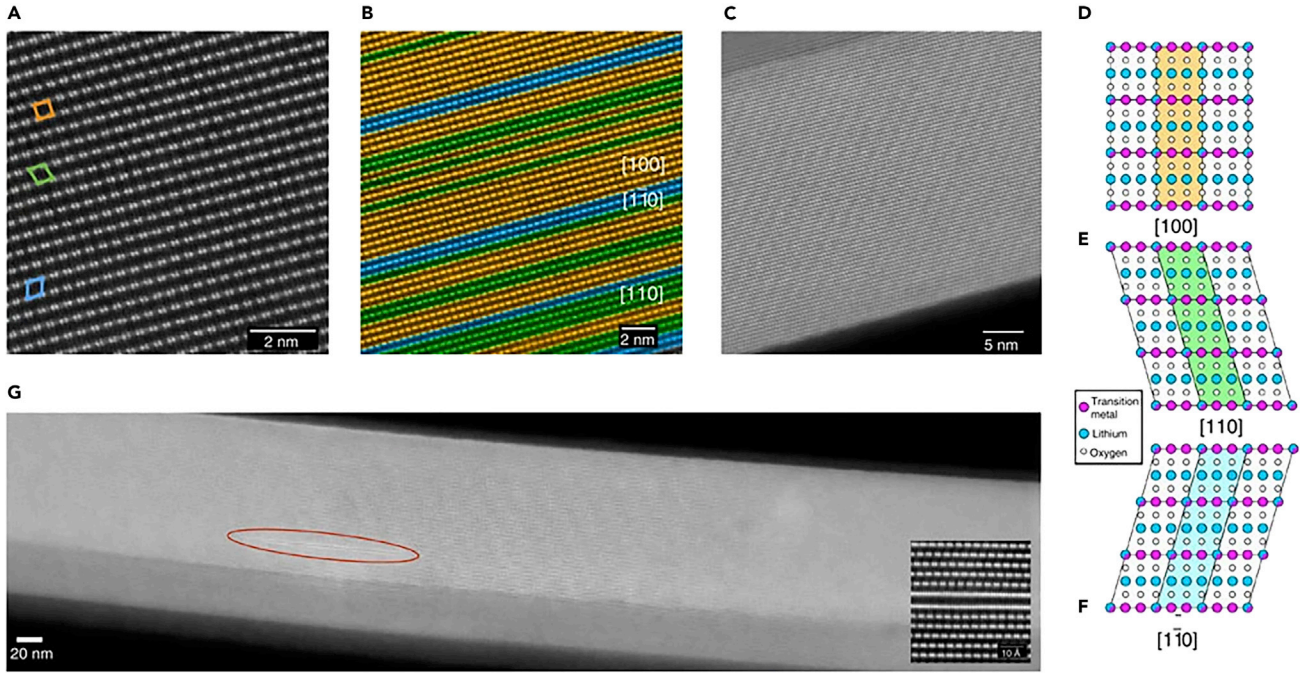

Figure 7. Experiments Illustrating the Single-Phase Nature of the Li-Rich Layered Materials

(A) HAADF image of a $Li_{1.2}Ni_{0.13}Mn_{0.54}Co_{0.13}O_2$ particle. The three colored boxes show the monoclinic variants.

(B) HAADF image of (A), colored to show the variations of the three monoclinic phases.

(C) HAADF image of a $Li_{1.2}Ni_{0.13}Mn_{0.54}Co_{0.13}O_2$ particle at a larger field of view.

(D–F) Schematic illustration of the crystal structure of the three monoclinic variations in a single particle of $Li_{1.2}Ni_{0.13}Mn_{0.54}Co_{0.13}O_2$.

(G) HAADF image of the entire primary particle shows that only one phase is present. The marked region in red and the corresponding inset show the occasional transition-metal-rich defects observed in the particle. Adapted from Shukla et al.[71]

made from O K-edge and TM L-edges from soft XAS, which, as mentioned before, cannot probe the localized hole states on the O 2p orbitals. Hence, a conclusive claim on oxygen redox in conventional layered materials could not be reached. However, recent studies showed that oxygen redox could be achieved in conventional layered materials at very high states of charge (SOCs).[24,33,79] In Ni-based layered oxides, Ni in +3 oxidation state has an electronic configuration of $3d^7(t_{2g}^6\ e_g^1)$ with partially filled e_g orbital, which means electron removal will first take place from the e_g orbital. Hence, electron removal from O 2p orbital will take place later at high SOCs.[80,81] This might give an indication of the high-voltage behavior of many technologically significant Ni-rich layered NMC materials ($LiNi_xCo_yMn_{1-x-y}O_2$), since $LiNiO_2$ can be taken as the parent material for this series of materials. Besides, high-voltage charging pushes the O 2p states closer to the Fermi level, making them redox active.[82] Utilizing RIXS on these materials at high SOCs allowed deciphering of the localized hole states in the O 2p orbitals contributing to the capacity at high voltages.

Oxygen Redox in Alkali-Poor Layered Transition Metal Oxides

The work of Ceder and coworkers has established the Li-O-Li configuration as an important structural descriptor to trigger oxygen redox in Li cathodes.[15] Such a descriptor can be obtained in large quantity in Li-rich layered oxides and DRX materials. In Li-rich DRX materials there are different oxygen sublattices, some of which have the Li-O-Li configuration because of the disordering of the transition metal cations, whereas in Li-rich layered materials the excess Li sitting in the transition metal layer enables the formation of the Li-O-Li configurations.[15] Sodium layered cathodes

provide a unique scenario with respect to oxygen redox and the alkali stoichiometry. Unlike their Li counterparts which largely form O3-type structures, sodium layered cathodes can be synthesized in different polymorphs (such as O3, P2, and P3).[83] O3 structure is empirically stabilized when the Na stoichiometry is close to 1 in Na_xTMO_2.[84,85] The P2 and P3 polymorphs are stabilized in sodium-poor stoichiometry (x is less than 1 in Na_xTMO_2).[86] Na-rich stoichiometry is attainable with 4d (e.g., Ru)[67] and 5d (e.g., Ir)[69] transition metals because of the smaller size difference between Na ion, and Ru or Ir ions. Hence, the Na-O-Na configuration can be found in sodium transition metal oxides with 4d and 5d transition metals, and oxygen redox has been reported in these materials.[68,69,87] However, for the case of sodium layered oxides with 3d transition metals (e.g., Ti, Cr, Mn, Fe, Co, Ni, Cu), the larger size difference between the transition metal ion and the Na ion does not allow the Na ion to stably occupy the transition metal layer.[83,88] Hence, attainment of the Na-O-Na configuration is not favored in sodium layered oxides with 3d transition metals. However, the almost similar size of Li ion and Mg ion compared with the transition metal ions allows them to replace some 3d transition metal ions in the transition metal layer.[43,49,89] Hence, the formation of Na-O-Li or Na-O-Mg configuration becomes possible. O 2p orbitals in these configurations are also expected to be unhybridized and, thus, redox active.[90] Additionally, cation vacancies are reported to increase the O 2p lone pair electrons and can trigger oxygen redox in alkali-poor sodium layered materials,[26] such as $Na_{2/3}[Mn_{0.72}Mg_{0.28}]O_2$[91] and $Na_{4/7}[\square_{1/7}Mn_{6/7}]O_2$.[92]

$Na_x[Li_yTM_{1-y}]O_2$[32,50] and $Na_x[Mg_yTM_{1-y}]O_2$[43,49] (where x is less than 1) are two examples of materials in which the oxygen redox is triggered without excess alkali and by substituting transition metals by either Li ion or Mg ion. Indeed, the presence of Li ion and Mg ion in the transition metal layer is well characterized in these materials. Structural characterization such as XRD, neutron diffraction, and Li-nuclear magnetic resonance (NMR) can give direct evidence of the specific lattice sites Li and Mg can occupy in these materials.[93–95] Combined XRD and neutron diffraction analysis with Rietveld refinement in P2–$Na_{0.66}Li_{0.18}Fe_{0.12}Mn_{0.7}O_2$ indicated the occupancy of Li in the transition metal layer (Figures 8A and 8B). An in-plane Li/TM ordering can be defined by a $\sqrt{3}a \times \sqrt{3}a$ supercell in this material.[89] The ordering is similar to typical honeycomb ordering of Li/Mn observed in Li-rich materials.[96,97] The honeycomb ordering can be assumed by alkali/alkaline-ion substitution in the transition metal layer, as shown in Figure 8D. Li-NMR can provide information of Li occupancy in the transition metal layer, e.g., in Li-substituted P2–$Na_{0.78}Li_{0.25}Mn_{0.75}O_2$ by a characteristic shift at 1,850 ppm (Figure 8C).[49]

Direct participation of oxygen to redox reactions has been documented in $Na_x[Li_yTM_{1-y}]O_2$ and $Na_x[Mg_yTM_{1-y}]O_2$ through various spectroscopic techniques. A reversible oxygen redox was observed in $Na_{0.6}[Li_{0.2}Mn_{0.8}]O_2$ through RIXS by a characteristic increase in the intensity at 531-eV excitation energy and a corresponding 523.7-eV emission energy (boxed region in Figure 9A).[32] Bruce and coworkers reported a change in spectral weight in O K-edge at high SOCs in $Na_{2/3}[Mg_{0.28}Mn_{0.72}]O_2$, indicative of oxygen redox (Figures 9B and 9C).[43] The O K-edge spectral evolution studied in alkali-poor cathode materials is similar to oxygen redox active Li-rich cathode materials reported in the literature.[28,30]

Recently, Yang and coworkers reported the contribution of oxygen redox in charge compensation of layered $Na_{2/3}Ni_{1/3}Mn_{2/3}O_2$ during cycling.[23] The oxidation of oxygen anion is particularly observed during the 4.2-V plateau on charging. This oxygen redox activity is fundamentally distinct from the other sodium layered oxides where transition metals are substituted with Mg and Li. The oxidation of oxygen anion at

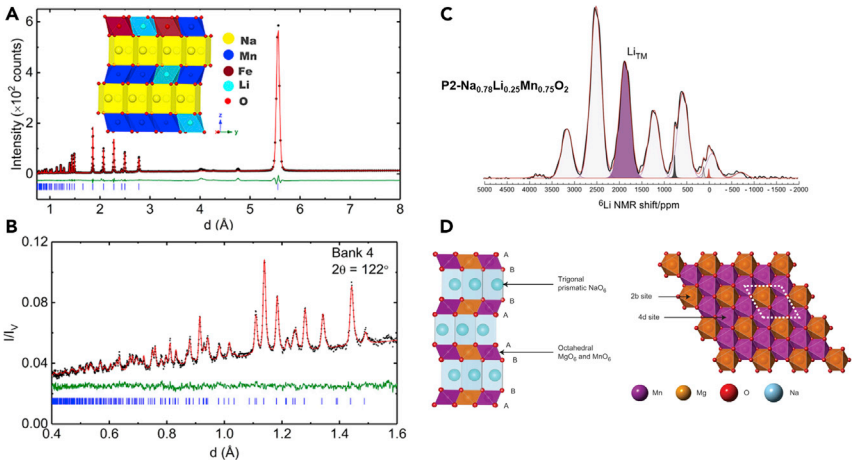

Figure 8. Structural Characterization of $Na_x[AM_yTM_{1-y}]O_2$ (where AM Is an Alkali/Alkaline Ion such as Li^+ or Mg^{2+}, and TM Is Transition Metal Ion), Showing that Alkali/Alkaline Ion Can Be Incorporated onto the Transition Metal Layer of the Sodium Layered Oxides

(A and B) (A) Synchrotron XRD pattern with Rietveld refinement and (B) neutron diffraction pattern with Rietveld refinement of P2–$Na_{0.66}Li_{0.18}Fe_{0.12}Mn_{0.7}O_2$. Adapted from Yang et al.[89]

(C) ^{6}Li-NMR of P2–$Na_{0.78}Li_{0.25}Mn_{0.75}O_2$, showing the presence of Li in the transition metal layer. Adapted from House et al.[49]

(D) Schematic crystal structure of $Na_{2/3}[Mg_{0.28}Mn_{0.72}]O_2$ showing the honeycomb ordering of Mg/Mn. Adapted from Maitra et al.[43]

high voltage can be similar to the oxygen redox activity observed in conventional stoichiometric layered oxide materials (see Mechanisms of Oxygen Redox and Oxygen Redox in Conventional Layered Transition Metal Oxides for more details).

Oxygen Redox in Disordered Rocksalt Oxides

Li-rich cation-DRX materials have opened up a vast compositional space to explore new Ni/Co free high-energy cathode materials for Li-ion batteries. These materials can utilize combined cationic and anionic redox chemistry to deliver large discharge capacity and energy density. DRX materials have a face-centered cubic structure. Normally, these materials do not have an open percolation network for Li insertion/de-insertion. However, having a Li-rich stoichiometry opens up a continuous percolation network for Li ions and allows for electrochemical cycling of Li ions.[19] In DRX materials, the Li percolation takes place by hopping of the Li ion from one octahedral site to another octahedral site through an intermediate tetrahedral site (Figure 10A). Li ion in the tetrahedral site is regarded as an active Li for the hopping. In DRX materials, since many oxygen sublattices exist, the intermediate tetrahedral site for the Li hopping can be face sharing with no-TM (0-TM in Figure 10B), 1-TM (Figure 10C), or 2-TM (Figure 10D) octahedral sites.[19] The electrostatic repulsion between a Li in the tetrahedral site and the surrounding octahedral TM can indicate whether one tetrahedral site will be feasible for Li percolation. The height of the tetrahedral site (about 2.35–2.45 Å) can be taken as a measure of the activation energy required for Li hopping. Owing to the small height of the tetrahedral site, the 1-TM channel in DRX materials has an activation energy of Li hopping of more than 500 meV and is usually inactive for Li hopping. However, these 1-TM channels are active for Li hopping in ordered layered transition metal oxides because of the larger interslab distance. Hence, only 0-TM channels are active for Li percolation in DRX materials. For macroscopic Li-ion conduction, a continuous network of these 0-TM channels is required. Monte Carlo simulations showed the critical Li concentration for the formation of sufficient 0-TM channels in DRX

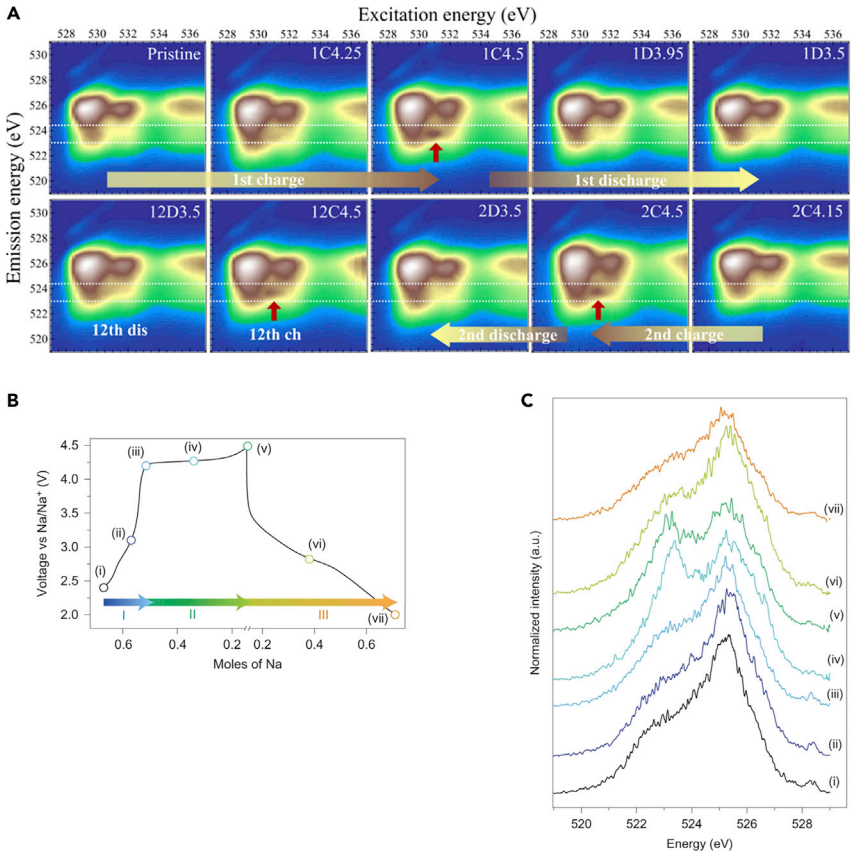

Figure 9. Probing Oxygen Redox in $Na_x[Li_yTM_{1-y}]O_2$ and $Na_x[Mg_yTM_{1-y}]O_2$ Type Materials

(A) Oxygen redox probed through RIXS at different states of charge in $Na_{0.6}[Li_{0.2}Mn_{0.8}]O_2$.

(B) First-cycle charge-discharge curves of $Na_{2/3}[Mg_{0.28}Mn_{0.72}]O_2$. The points on the curve indicate the states of charge where RIXS spectra were collected in (C).

(C) O K-edge RIXS spectra at different states of charge on the first cycle of $Na_{2/3}[Mg_{0.28}Mn_{0.72}]O_2$. Adapted from Wu et al.[32] and Maitra et al.[43]

materials for continuous macroscopic Li diffusion.[98] Figure 10E shows the periodical wrapping probability for various combinations of percolation channels in DRX materials. A cluster of sites are periodically wrapping if the cluster has different periodic images of the same Li site. Since 0-TM channels are likely to be the main percolation channels for DRX materials, it can be seen from Figure 10E that at least 10% Li-excess composition is required for the 0-TM channels to percolate Li ions (red dashed line). Furthermore, the fraction of accessible Li ions from the DRX materials for electrochemical cycling increases with increasing Li composition. For at least one accessible Li per formula unit, an excess of 25% Li in the composition is required (red dashed line and black horizontal line in Figure 10F). Hence, this shows that excess Li composition is required for DRX materials to electrochemically cycle Li ions. The rule of thumb of excess Li composition can be applied to most DRX materials and is independent of the type of the transition metal ions. Disordering of the transition metals in the rocksalt structure is facilitated with transition metals of d^0 electronic configuration while transition metals with d^6 electronic configuration prohibit disordering.[99] Cation disordering can affect the properties of cathode materials such as Li-ion conductivity. For example, in $Li_{1.2}Mn_{0.4}Zr_{0.4}O_2$, the short-range cation ordering leads to significantly less Li-ion conductivity than in more disordered $Li_{1.2}Mn_{0.4}Ti_{0.4}O_2$.[100]

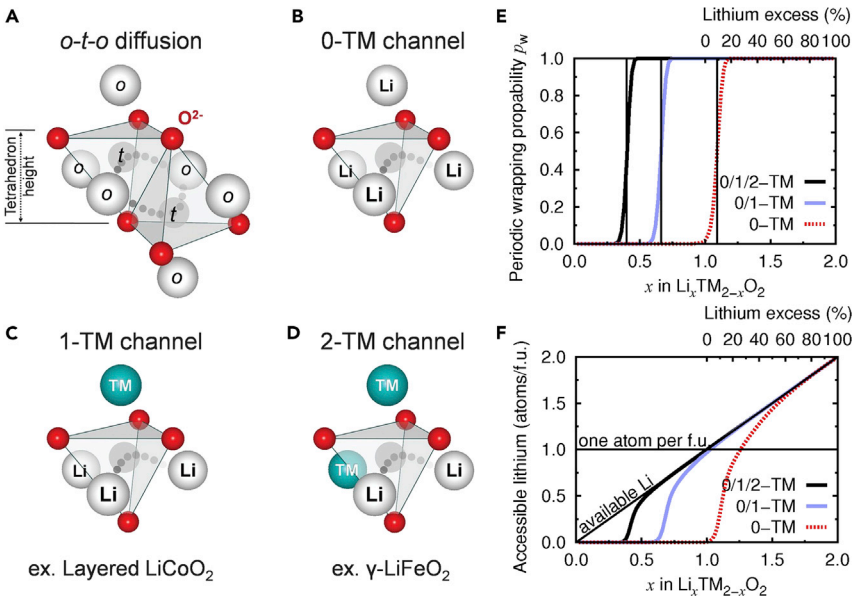

Figure 10. Formation of Li Percolation Network in Disordered Rocksalt Materials

(A–F) (A) Schematic illustration of the octahedral-tetrahedral-octahedral (o-t-o) hopping of Li ion. (B–D) The local environment of the intermediate tetrahedral site. The tetrahedral site is surrounded by (B) no transition metal, (C) one transition metal, and (D) two transition metals. Adapted from Lee et al.[19]

(E and F) Li-excess stoichiometry for open percolation network in disordered rocksalt materials. Periodic wrapping probability (E) and accessible Li content against the overall Li content of the material (F). An excess Li stoichiometry is required for DRX materials to macroscopically conduct Li ions. Adapted from Urban et al.[98]

Because of the disordered nature of the cation distribution in DRX materials, there can be significant numbers of Li-O-Li configurations,[15] and some oxygens may have more than one Li-O-Li configuration (e.g., the local Li-rich environment such as that in 0-TM channels).[98] Hence, oxygen redox activity is expected in these materials.[101] Indeed, Yabuuchi et al. reported disordered $Li_{1.3}Nb_{0.3}Mn_{0.4}O_2$ with large discharge capacity due to the combined cationic and anionic redox activities.[20] The authors of this study performed partial density of states (pDOS) calculation on the material with the general formula $Li_{(4-y)/3}Mn_{1/3}Nb_{1/3}O_2$ ($0 \leq y \leq 4$) to understand the participation of oxygen on charge compensation (Figure 11). Charge compensation in this material at the initial y values (0–1) takes place mainly from the Mn e_g orbitals of the MnO_6 octahedra according to the calculated density of states from the top of the valence band at $y = 0$ and the bottom of the conduction band at $y = 1$ (green circles on the right panel of Figure 11 for the y values 0–1). For the y values 1–3, O 2p orbitals mainly take part in redox reaction as can be seen from the top of the valence band at $y = 1$ (blue circle in the right panel of Figure 11) and the bottom of the conduction band at $y = 2$, 3 (blue circles on the right panel of Figure 11), and they are mainly composed of dumbbell-shaped O 2p orbitals. The drastic change in the density of states on the Mn e_g orbitals at higher SOCs ($y = 4$) indicates that further Mn oxidation can take place at deeper delithiation level. Lattice oxygen redox in DRX materials has also been substantiated by experimental evidence through techniques such as RIXS.[102–105] However, quite often the feature indicating lattice oxygen oxidation appears as only a shoulder because of the strong overlap of TM-4d states in second-row transition metal-containing DRX materials.[103] In addition, it has been reported that the lattice oxygen redox does not lead to distortion of the lattice oxygen framework with reduced O–O separation.[102] Due to the random distribution of the cations in DRX materials, the formation probability of coplanar unhybridized O

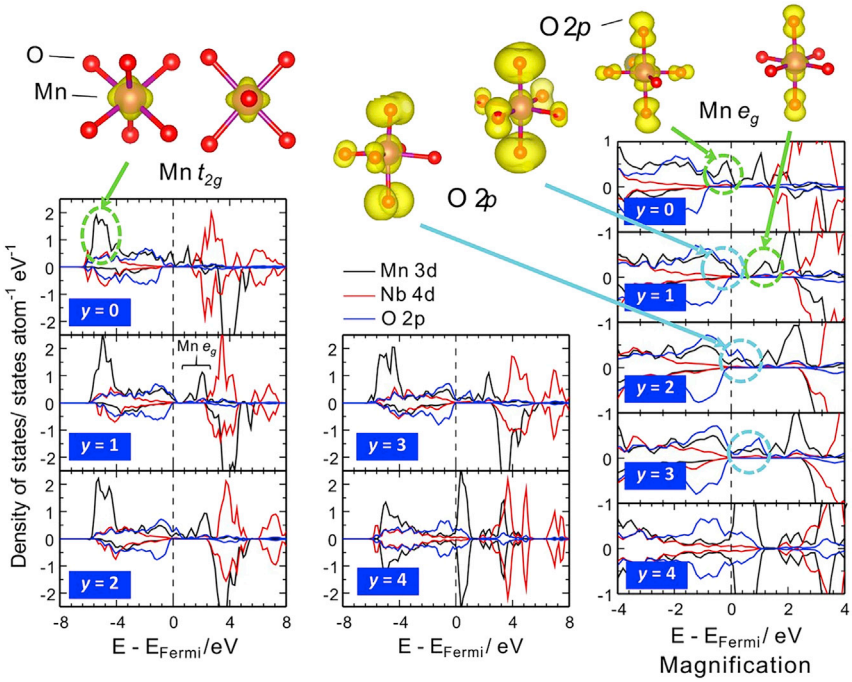

Figure 11. Understanding Charge Compensation of $Li_{(4-y)/3}Mn_{1/3}Nb_{1/3}O_2$ ($0 \leq y \leq 4$) through Partial Density of States and Partial Electron Density Calculation

The density of states calculation shows different participation of transition metal and oxygen to redox reactions during Li deintercalation. Adapted from Yabuuchi et al.[20]

2p orbitals greatly reduces, leading to the lesser interaction between the oxidized oxygens.

Utilizing a vast array of compositions, various DRX materials have been reported with large capacity and energy density.[20,106–109] Fluorine substitution strategy and incorporating d^0 transition metals with high valence states can keep the valence states of the redox active species low, thus enabling facile redox reactions of the redox active transition metal ions.[4,110–112] For example, the lower valence state of Mn achieved in $Li_2Mn_{2/3}Nb_{1/3}O_2F$ through the incorporation of high-valence-state Nb^{5+} and F substitution has enabled the use of Mn^{2+}/Mn^{4+} redox couple in this material.[113] In addition to a small amount of oxygen redox, this material can deliver more than 300 mAh/g discharge capacity and almost 1,000 Wh/kg discharge energy, although the lower cut-off voltage has to reach 1.5 V versus Li/Li^+. Due to the absence of specific ordering in DRX materials, these materials can utilize a wide variety of transition metals, which can be crucial for developing a cost-effective alternative to more conventional ordered lithium layered oxide materials with expensive Ni/Co as the transition metals.[4]

In summary, various cathode materials can utilize oxygen redox and transition metal redox to deliver high capacity. For the convenience of the reader, we have summarized below (Table 1) the capacity contribution of oxygen and transition metal redox during initial cycling when the data were reported in the literature.

ISSUES WITH OXYGEN REDOX

Voltage Hysteresis and Fading

Even though oxide cathodes showing oxygen redox are a promising group of materials due to their high discharge capacity, they present significant challenges toward

Table 1. Contribution of Oxygen Redox and Transition Metal to the Observed Initial Capacity of Various Cathode Materials (Li-Rich Oxides, Disordered Rocksalts, Li-Substituted Oxides, and Conventional Layered Oxides)

Material	Voltage Window (V)	Cycling Rate (mA/g)	Cationic Redox Capacity (mAh/g)	Anionic Redox Capacity (mAh/g)	Reference
$Li_{1.2}Ni_{0.13}Mn_{0.54}Co_{0.13}O_2$[a]–	2.0–4.8	20	141	123	Assat et al.[45]
$Li_{1.2}Ni_{0.15}Mn_{0.55}Co_{0.1}O_2$–	2.0–4.8	21	134	128	Hu et al.[30]
$Li_2Ru_{0.75}Sn_{0.25}O_3$–	2.0–4.6	32	120	120	Assat et al.[65]
$Li_{1.3}Mn_{0.2}Co_{0.1}Cr_{0.1}Ti_{0.1}Nb_{0.2}O_{1.7}F_{0.3}$–	1.5–4.7	20	175	132	Lun et al.[112]
$Li_{1.25}Nb_{0.25}Mn_{0.5}O_2$[b]–	1.5–4.8	10	146	141	Wang et al.[17]
$Na_{0.6}[Li_{0.2}Mn_{0.8}]O_2$–	3.5–4.5	10	66.6	8.8	Wu et al.[32]
$Na_{2/3}Ni_{1/3}Mn_{2/3}O_2$–	2.3–4.5	16	60.4	43.1	Dai et al.[23]

[a]Second-cycle capacity.
[b]Cycling performed at 55°C.

materials development, which has hindered their practical applications.[114] Voltage hysteresis and fading, and low initial Coulombic efficiency (Figure 12) are some of these challenges, which require further understanding and mitigation strategies.[115] A large voltage hysteresis, which refers to the difference in voltage between charge and discharge cycles, is especially observed in the first cycle. Voltage hysteresis leads to a decrease in energy efficiency and is persistent throughout the electrochemical cycling of most of the cathode materials with oxygen redox. The continuous decrease of the average discharge voltage referred to as voltage fading renders subpar energy output even when the capacity is not fading drastically.[115] Meanwhile, the low first-cycle Coulombic efficiency indicates irreversible structural and chemical transformations.[116] In general, some of the reasons behind voltage fading include but are not limited to (1) irreversible transition metal migration,[32,39,117,118] (2) emergence of new redox couples,[30] and (3) oxygen evolution.[26,101] Often these processes are interconnected; for example, irreversible oxygen evolution can cause irreversible transition metal migration and associated structural changes.[101,119,120] Meanwhile, some of the reasons behind the particularly severe voltage hysteresis between the first charge and first discharge have been attributed to the following: (1) charge-transfer band gap,[121] (2) asymmetric redox couple evolution,[28] (3) sluggish nature of oxygen redox,[29] and (4) type of ordering of alkali-ion/transition metal ion in the transition metal layer.[41]

Tarascon and coworkers reported out-of-plane transition metal migration to the Li layer in $Li_2Ru_{0.75}Ti_{0.25}O_3$.[117] The migration can take place from one octahedral site to another through an intermediate tetrahedral site. Such migration is reported to be reversible to some degree, but the migrated transition metal can get entrapped in the tetrahedral site on repeated cycling. The entrapment of the transition metal ions in the tetrahedral site has been attributed to the continuous voltage fading of $Li_2Ru_{0.75}Ti_{0.25}O_3$.[117] The study by Chueh and coworkers showed that transition metal migration to the Li layer is necessary for triggering and stabilizing oxygen redox in materials such as $Li_{2-x}Ir_{1-y}Sn_yO_3$, even though such migration may lead to voltage hysteresis.[39] An out-of-plane migration of Sn to the Li site creates a point defect on the transition metal layer and significantly changes the electronic structure of the material (Figure 13). Meanwhile, the migration of Sn is favored over Ir because of the stabilization effect of Sn on the delithiated structure (stabilization of 1.34–1.36 eV by Sn migration against a stabilization of 0.02 eV by Ir migration). The authors predicted that upon the out-of-plane migration of Sn, one of the two outcomes can take place depending on the type of local structure from which Sn is migrating.

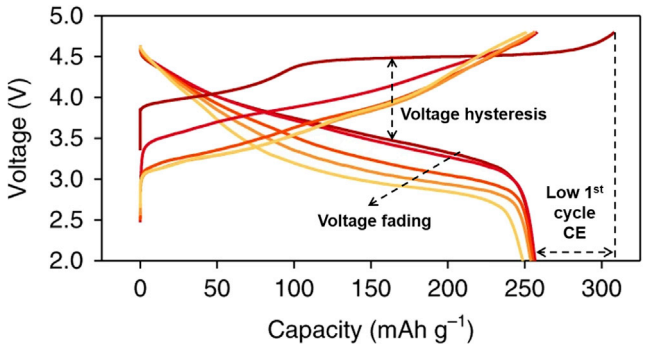

Figure 12. Voltage Hysteresis, Voltage Fading, and Low First-Cycle Coulombic Efficiency Observed in Li-Rich Cathodes with Oxygen Redox

The vertical dashed arrow between the charge and discharge curves indicate voltage hysteresis arising from the difference in voltage in charge and discharge cycle. The difference persists in subsequent electrochemical cycling. The black arrow across the discharge curves indicates the fading nature of the output voltage, even when the capacity is not fading drastically. CE, Coulombic efficiency. Adapted from Hu et al.[30]

If an Sn migrates from a site that was the nearest neighbor to an Ir in the transition metal layer, a substantial contraction of the Ir–O bond takes place (Figure 13A), which also leads to the splitting of the unhybridized O 2p states. A part of the split state moves above the Fermi level and becomes oxidized (shaded region in Figure 13B). The oxidized oxygen states above the Fermi level can rehybridize with Ir 5d states. The crystal orbital overlap population analysis performed by Chueh and coworkers indicates that the rehybridization can form a short Ir–O π bond through a ligand-to-metal charge-transfer process. However, if the migration of Sn takes place from a local structure where the nearest neighbor was another Sn atom (Figure 13C), the single coordinated oxygen atoms form an O–O dimer (1.44 Å bond length), which also results in reshuffling of the nonbonding O 2p states to above the Fermi level (Figure 13D). Meanwhile, the migration of Sn to the Li layer is argued to be initiated by the oxidation of Ir beyond 5.5+ state. In such a highly oxidized state, facile ligand-to-metal charge transfer can take place. The bonding and structural configurations that support this transfer are stabilized by such charge transfer. Hence, it is clear that the oxygen redox can trigger transition metal migration, which acts to stabilize the oxygen redox,[28] but the irreversible transition metal migration can lead to voltage fading on consecutive cycling.

Meanwhile, Hu et al. reasoned the emergence of new redox couples such as Co^{2+}/Co^{3+} and Mn^{3+}/Mn^{4+} due to oxygen loss and transition metal reduction on the observed voltage fading of $Li_{1.2}Ni_{0.15}Co_{0.1}Mn_{0.55}O_2$.[30] The emergence of these new redox couples raises the Fermi level and lowers the operating voltage because of the smaller difference between the Fermi level and the Li^0/Li^+ energy level (Figure 14). Such lowering of the operating voltage contributes to the voltage fading of the material. Similar to this observation, Yang and coworkers attributed the voltage fading of P2–$Na_{0.6}[Li_{0.2}Mn_{0.8}]O_2$ to the increasing contribution of Mn redox on cycling.[32]

Assat et al. evaluated the electrochemical reaction mechanism of $Li_{1.2}Ni_{0.13}Mn_{0.54}Co_{0.13}O_2$ in detail and revealed that the oxygen redox reaction considerably slows down the electrochemical kinetics.[29] A detailed charge-compensation study revealed that small anionic activity and Mn^{3+}/Mn^{4+} redox is mainly observed on low potential charging (blue shaded region in Figure 15). Meanwhile, the capacity at charging to 4.1 V is predominantly obtained by the redox activity of $Ni^{2+/3+/4+}$ and $Co^{2+/3+}$ redox

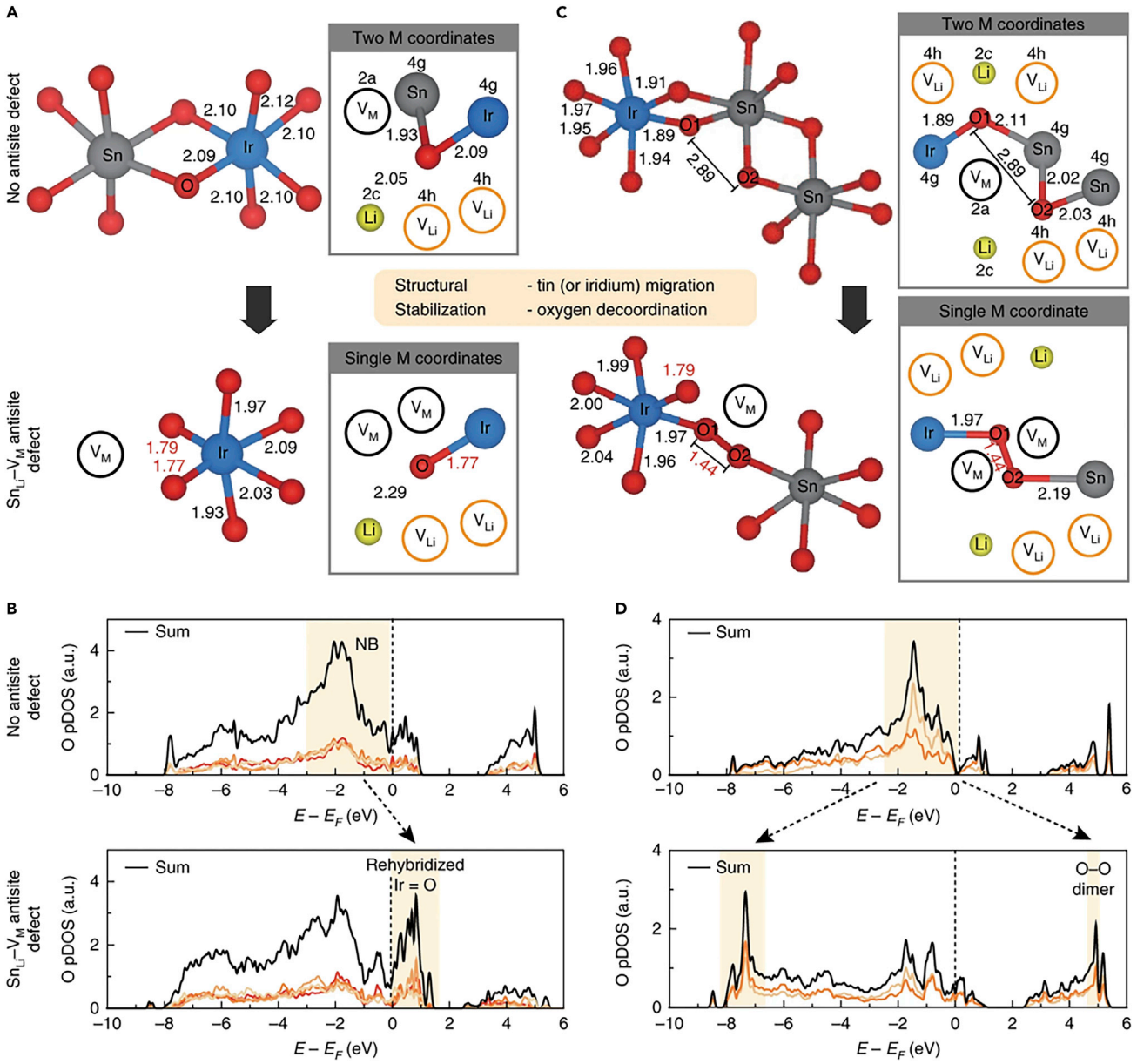

Figure 13. Computational Analysis of the Transition Metal Migration-Triggered Oxygen Redox Behavior in $Li_{0.5}Ir_{0.75}Sn_{0.25}O_2$ (Charged)

(A) Oxygen coordination environment (right) and Ir–O bond length (left) calculated by DFT before and after the Sn migration. The migrated Sn initially neighbors an Ir atom.

(B) Evolution of the electronic structure as calculated through the pDOS of oxygen before and after the Sn migration in (A).

(C) Oxygen coordination environment (right) and Ir–O bond length (left) before and after the Sn migration. The nearest neighbor of the migrated Sn is another Sn atom.

(D) Electronic structure evolution triggered by the migration of Sn neighboring another Sn atom (C) as calculated through pDOS of oxygen. Adapted from Hong et al.[39]

active species (gray shaded region in Figure 15). Charging to higher voltage (4.8 V), the charge compensation primarily takes place from the oxidation of O^{2-} (red shaded region in Figure 15). On subsequent discharge, O^{n-} ($n < 2$) reduces over two voltage regions: the high-voltage region (green shaded area in Figure 15), and low-voltage region (red shaded area with 3.2-V reduction peak in Figure 15). Such asymmetric oxygen redox evolution leads to voltage hysteresis.

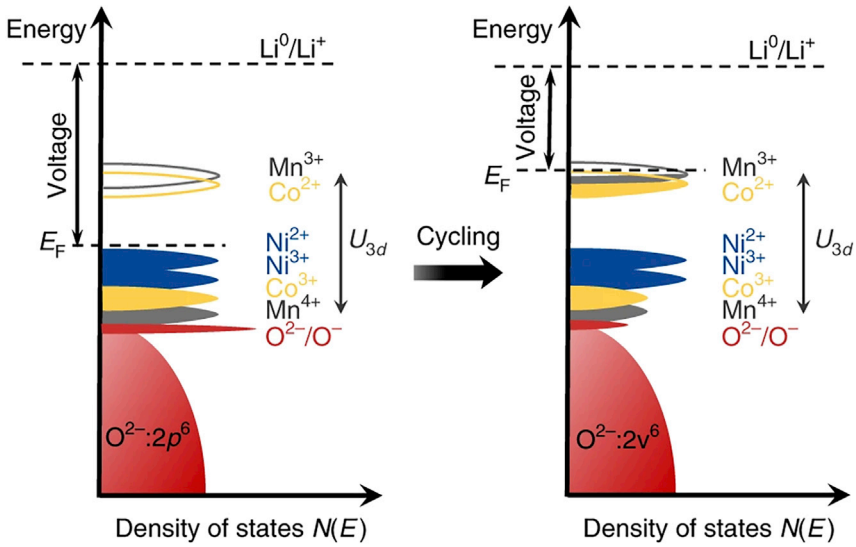

Figure 14. Effect of the Redox Couple Evolution on the Output Voltage of Li-Rich Layered Materials

Density of states in $Li_{1.2}Ni_{0.15}Co_{0.1}Mn_{0.55}O_2$ before cycling (left) and after cycling (right). Evolution of new redox couples such as Mn^{3+}/Mn^{4+} and Co^{2+}/Co^{3+} lowers the operating voltage. Adapted from Hu et al.[30]

Tarascon and coworkers proposed charge-transfer band gap as an indicator of voltage hysteresis.[121] The density of states calculation on the disordered $Li_{1.3}Ni_{0.3}Ta_{0.4}O_2$ shows that the material has a large Mott-Hubbard band gap. The band gap reduces to a small charge-transfer band gap on delithiation and before the onset of anionic oxidation (left panel of Figure 16B). After the onset of anionic oxidation, structural reorganization takes place, leading to the formation of O–O dimers with σ, π, σ*, and π* bands. Since the antibonding state such as σ* sits above the empty metal band, electron transfer from O to metal takes place, causing the reduction of transition metal and molecular oxygen evolution (left panel of Figure 16C). Such irreversible transformation leads to the large voltage hysteresis and fading in the cycling curves of $Li_{1.3}Ni_{0.3}Ta_{0.4}O_2$ (Figure 16D). On the other hand, after the onset of the anionic redox in $Li_{1.3}Mn_{0.4}Ta_{0.3}O_2$, the antibonding states stay below the metal band (right panel of Figure 16B) and electron transfer from oxygen to metal cannot take place, stabilizing the oxygen redox. Consequently, less voltage hysteresis is observed in $Li_{1.3}Mn_{0.4}Ta_{0.3}O_2$ (Figure 16D). Meanwhile, the smaller voltage hysteresis in $Na_{0.6}[Li_{0.2}Mn_{0.8}]O_2$ as compared with $Na_{0.75}[Li_{0.25}Mn_{0.75}]O_2$ was attributed to the differences in Li/Mn ordering in the transition metal layer of these two materials (Figures 16E and 16F).[41] $Na_{0.75}[Li_{0.25}Mn_{0.75}]O_2$ shows honeycomb-type ordering, which is not effectively maintained on cycling (Figure 16E). $Na_{0.6}[Li_{0.2}Mn_{0.8}]O_2$ shows ribbon-type ordering that is well maintained (Figure 16F), leading to less voltage hysteresis.

It is clear that a host of reasons have been related to the voltage hysteresis and voltage fading of materials showing oxygen redox. It is thus most reasonable to mention the underlying reasons behind voltage hysteresis/fading as materials specific. However, there seems to exist a strong correlation between transition metal migration and voltage hysteresis and fading. Reversible transition metal migration may lead to voltage hysteresis, but irreversibility in transition metal migration will lead to voltage fading.[122] In some materials, oxygen redox itself due to slow redox kinetics and asymmetric redox evolution has been attributed to voltage hysteresis,

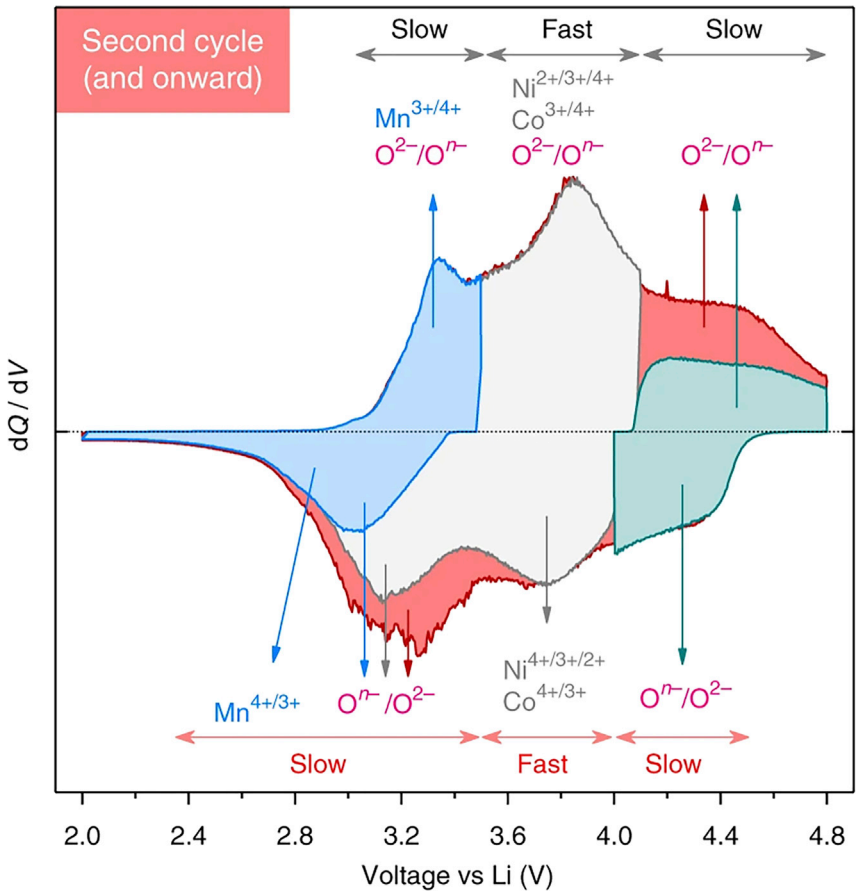

Figure 15. Charge-Compensation Mechanism and Electrochemical Kinetics of $Li_{1.2}Ni_{0.13}Mn_{0.54}Co_{0.13}O_2$ beyond the First Cycle

Predominant charge compensation takes place through oxygen redox when charged to 4.8 V. On discharge, oxygen reduces in two potential ranges: high potential region (green shaded region) and low potential region (red shaded region). Adapted from Assat et al.[29]

even when no appreciable transition metal migration is observed.[43] Indeed, voltage hysteresis has been observed to increase when anionic redox chemistry is involved.[29] Oxygen redox is usually kinetically slow and causes voltage hysteresis on electrochemical cycling. The structural and electronic reorganization that ensued after stabilization of the oxygen redox may also be responsible for the voltage hysteresis.[118,123] Such reorganization caused by the oxygen redox may alter the sequence of cationic and anionic redox reactions (e.g., cationic-to-anionic oxidation on charge followed by cationic-to-anionic reduction on discharge) and cause voltage hysteresis.[30] Meanwhile, irreversible oxygen redox in the form of oxygen evolution may lead to a cation-densified state as a result of irreversible transition metal migration. The accumulation of the irreversible transition metal migration may lead to voltage fading. Irreversible oxygen redox can also lead to transition metal reduction, which causes emergence of new redox couples. Contribution of some of these redox couples such as Co^{3+}/Co^{4+} and Mn^{3+}/Mn^{4+} can lower the output voltage during cycling, causing voltage fading.[30]

Irreversible Oxygen Redox and Oxygen Evolution

Irreversible oxygen redox and oxygen evolution are commonly observed because of the reactive nature of the oxidized oxygen. The irreversibility associated with the

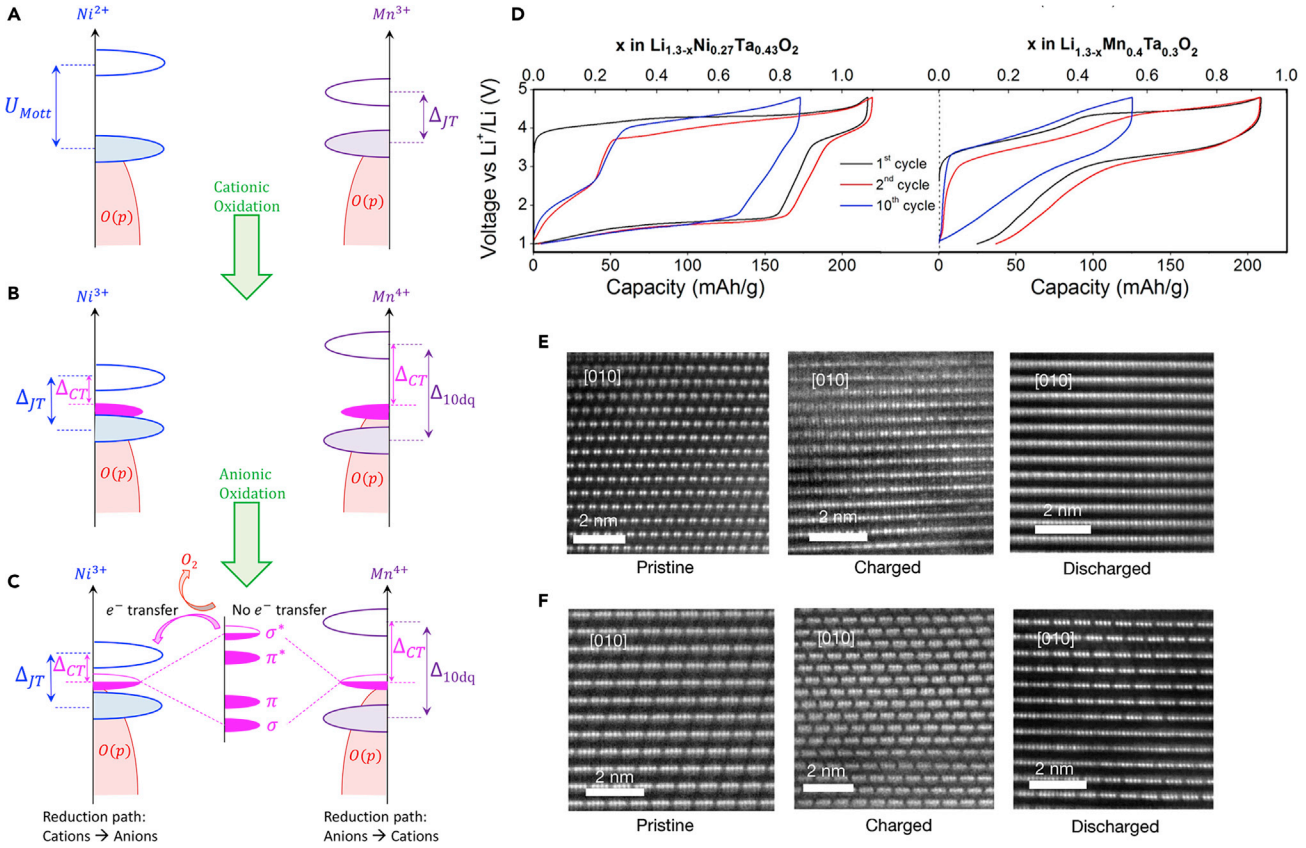

Figure 16. Charge-Transfer Band Gap and Superstructure Control as Indicators of Voltage Hysteresis on Materials with Oxygen Redox

(A–C) (A) Electronic band structure (calculated through the density of states) of $Li_1Ni_{0.3}Ta_{0.4}O_2$ (left) and $Li_{1.3}Mn_{0.4}Ta_{0.3}O_2$ at the pristine state (right), (B) during cationic oxidation, and (C) during anionic oxidation.

(D) Charge and discharge curves of $Li_{1.3-x}Ni_{0.27}Ta_{0.43}O_2$ (left) and $Li_{1.3-x}Mn_{0.4}Ta_{0.3}O_2$ (right). Adapted from Jacquet et al.[121]

(E) Honeycomb ordering in P2–$Na_{0.75}[Li_{0.25}Mn_{0.75}]O_2$ studied through STEM-ADF images along the [010] zone axis. Adapted from House et al.[41]

(F) Ribbon ordering in P2–$Na_{0.6}[Li_{0.2}Mn_{0.8}]O_2$ studied through STEM-ADF images along the [010] zone axis. Adapted from House et al.[41]

O^{2-}/O^- redox couple might lead to permanent structural modifications,[118,124–126] oxygen gas evolution,[127–131] and accelerated electrolyte decomposition through the nucleophilic attack of the oxidized oxygen with the electrolyte.[29,103] Oxide ion in the oxidized state can either form O–O dimers through structural reorganization, or the hole states can be localized in the unhybridized O 2p orbitals.[23,26,43,132] The O–O bonds are kinetically labile toward oxygen evolution.[133] Meanwhile, if the hole formation in the O 2p orbitals is not stabilized, it can lead to oxygen release and accelerated electrolyte decomposition. Indeed, the migration barrier of the oxidized oxygen is found to be significantly lower than that of O^{2-}, which may contribute to the irreversibility of the oxygen redox.[134,135] Meanwhile, in conventional Li/Na layered materials the oxygen stability is closely related to the SOC.[120,136,137] At higher SOCs, O_2 and CO_2 evolution is observed in $LiCoO_2$.[138,139] The thermal stability of the delithiated Li_xCoO_2 ($x < 1$), which can indicate the oxygen stability, decreases significantly in comparison with the pristine $LiCoO_2$.[139] The thermal stability is also compromised in delithiated Li-rich materials.[140] Ni-rich layered materials are also prone to irreversible oxygen redox and associated structural transformations.[141] Ni can form facile antisite defects with Li in layered materials, and the process is accelerated at high SOCs.[9,10] Such migration can lead to structural transformation (layered to spinel/rocksalt) and lead to oxygen release.[119] The instability of the Ni ions at high valence states is particularly severe because of the thermodynamic

instability of the Ni e_g electrons.[139] Various spectroscopic techniques such as RIXS,[24,48,50,142,143] XAS,[48,144,145] and XPS are utilized to probe the reversibility of oxygen redox.[27,94] Meanwhile, DEMS has allowed the direct study of the nature of irreversible oxygen redox in cathode materials (see Oxygen Redox in Alkali-Rich Layered Transition Metal Oxides for more details).[146–148] A combined analysis with DEMS and spectroscopic techniques such as RIXS, XAS, or XPS allows the study of the whole range of oxygen redox whether reversible or irreversible. Gasteiger and coworkers showed the evolution of singlet oxygen from Li-rich NMC materials at high SOCs through emission spectroscopy and CO and CO_2 evolution through on-line mass spectrometry.[149] This further signifies the reversible and irreversible nature of oxygen redox observed in these materials.

Structural and Chemical Evolution in Irreversible Oxygen Redox

A gradual structural and chemical transformation triggered by irreversible oxygen redox is usually observed in materials where oxygen plays a significant role in redox reactions.[118] In the literature where Li-rich materials are reported as a composite of Li_2MnO_3 and layered $LiMO_2$, Li_2O (lithia)-like structural units are claimed to be extracted at high-voltage charging.[14,54] Such irreversible Li and oxygen extraction is accompanied by structural transformations from layered to cation-dense structures (spinel and rocksalt). The origin of structural transformations may be involved with irreversible transition metal migration to the Li site, led by oxygen extraction.[150] A transition metal ion surrounded by five oxygens instead of six due to the oxygen release will be destabilized and move toward the vacant octahedral site of the Li layer.[151] Structural transformation in Li-rich materials from layered to spinel to rocksalt is observed, which is more severe at the surface region of the particle.[119,151–154] Boulineau et al. studied the surface structural reorganization of $Li_{1.2}Mn_{0.61}Ni_{0.18}Mg_{0.01}O_2$ at different C-rates and cycle numbers (Figure 17).[151] The pristine material can be defined as a well-ordered layered structure with a homogeneous distribution of the transition metals from the surface to the bulk (Figure 17A). However, on prolonged cycling (50 cycles at C/10 rate), a thick reconstructed surface layer emerges, which is composed of defective spinel structure with an outer layer of rocksalt (Figure 17B). Moreover, segregation of transition metal is observed with a higher ratio of Ni at the surface region of the particle in comparison with the bulk (Figure 17B). Such segregation indicates that the surface reconstruction takes place mostly through the migration of the Ni ions. Ni at higher oxidation state (close to +4) is thermodynamically unstable, triggering the migration of Ni ions to the vacant Li sites.[139] Meanwhile, a gradual loss of the superstructure reflection on cycling in the XRD pattern (Figure 17C) indicates progressive disordering of Li and transition metal ions, consistent with the transition metal migration observed in STEM images. Usually the migrated transition metal ions in the Li site are in the reduced state compared with the transition metal ions in the transition metal site (Figure 17D).[119,153] Since the reconstructed layer is a few nanometers thick and mostly limited to the surface, the oxidation state of the transition metals underneath the surface reconstruction layer is higher (Figure 17D).

Oxygen release can cause mechanical degradation of cathode particles. Mu et al. studied the chemomechanical degradation of layered $Li_{1-x}Ni_{0.4}Mn_{0.4}Co_{0.2}O_2$ (NMC) particles caused by irreversible oxygen release under thermal abuse conditions.[120] The authors performed an *in situ* TEM study at 230°C of the delithiated NMC particles in order to accelerate the oxygen release and associated chemomechanical evolutions. Z-contrast STEM images were recorded to observe the nucleation and propagation of cracks at the primary particle level (Figure 18). After a short incubation period of

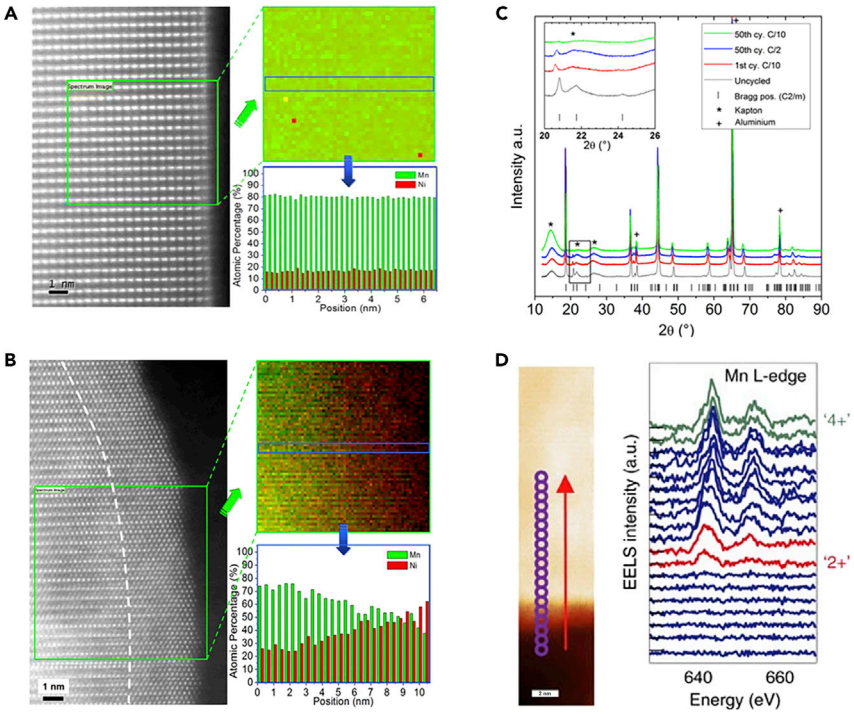

Figure 17. Structural and Chemical Evolution in Layered Cathodes Triggered by Irreversible Oxygen Redox

(A) HAADF-STEM image of pristine $Li_{1.2}Mn_{0.61}Ni_{0.18}Mg_{0.01}O_2$ (left) and the EELS concentration map and histogram (right) of the boxed region on the STEM image.

(B) HAADF-STEM image after 50 cycles at C/10 rate (left) and the EELS concentration map and histogram (right) of the boxed region on the STEM image.

(C) XRD pattern of $Li_{1.2}Mn_{0.61}Ni_{0.18}Mg_{0.01}O_2$ before and after cycling at various C-rates and cycle numbers. Adapted from Boulineau et al.[151] Chemical evolution on the surface reconstruction of $LiNi_{0.4}Mn_{0.4}Co_{0.18}Ti_{0.02}O_2$.

(D) STEM image highlighting the regions (in circles) in which EELS spectra were acquired (left) and Mn L-edge EELS spectra on the marked regions of the STEM image (right). Adapted from Lin et al.[119]

about 7 min, several microcracks grew quickly in length up to 15 min and grew slowly afterward (about 90 nm after 40 min). Such chemomechanical degradation in practical electrodes can lead to several other phenomena such as detachment of the cathode particle from the binder matrix,[155] transition metal dissolution, accelerated cathode-electrolyte side reactions,[141] and poor electronic conductivity.[156] All of these processes combined can step up the overall degradation of the cathode material.

STABILIZATION OF OXYGEN REDOX AND MITIGATION OF THE STRUCTURAL/CHEMICAL IRREVERSIBILITY

Suppressing Voltage Hysteresis and Fading

Voltage hysteresis and fading are major roadblocks to the development of high-energy Li-rich layered materials. Many mitigation strategies to suppress voltage hysteresis and fading have been reported. These methods include cation doping,[157] tuning crystal structure,[158] controlling redox couple evolution,[32] compositional control,[159,160] gradient Li distribution,[161] and tuning the non-electroactive cathode component.[162] Here we summarize these strategies.

Tuning the crystal structure of $Li_x(Li_{0.2}Ni_{0.2}Mn_{0.6})O_2$ from an O3 to an O2 type has resulted in suppression of voltage fading on long-term cycling and minimum initial

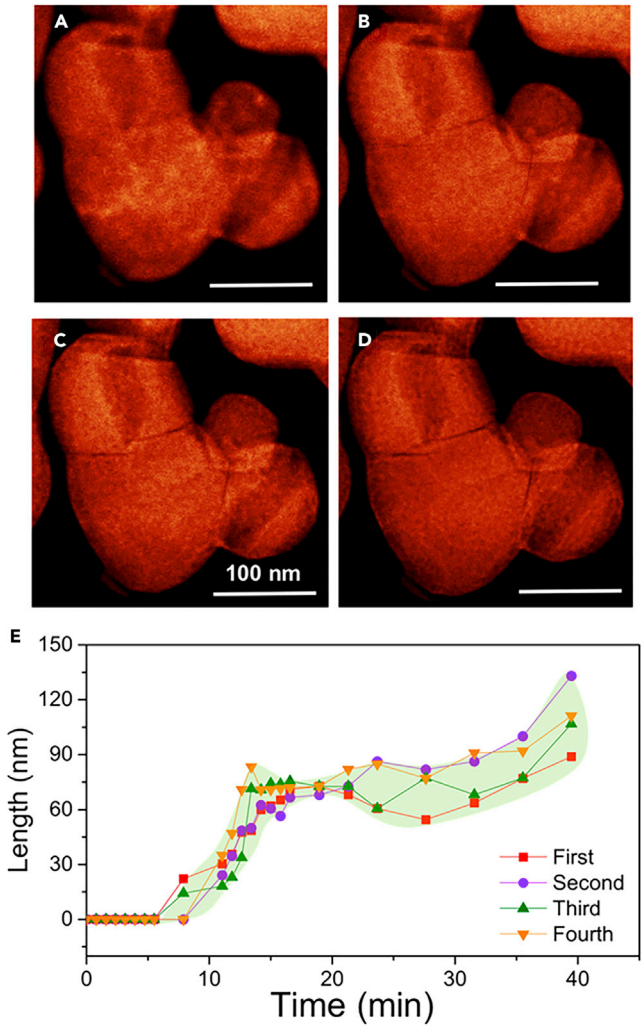

Figure 18. Chemomechanical Degradation of Layered Materials due to Irreversible Oxygen Loss
(A–D) Evolution of cracks monitored through selective Z-contrast STEM images upon heating $Li_{0.5}Ni_{0.4}Mn_{0.4}Co_{0.2}O_2$ at 230°C for (A) 0 min, (B) 12 min, (C) 26 min, and (D) 40 min.
(E) Growth of cracks over time. Four cracks are individually measured and plotted. The initial growth of microcracks is rapid during heating, which slows down with time. Adapted from Mu et al.[120]

voltage hysteresis.[158] For the O2-type structure, TMO_6 octahedra in the transition metal layer is face shared with the LiO_6 octahedra in the Li layer (Figure 19B). Transition metal migration from an intermediate tetrahedral site to an octahedral site of the Li layer is not favored because of the electrostatic repulsion between the cations in the face-shared octahedral sites (Figure 19B). The authors argue that the large electrostatic repulsion encourages the transition metal ions in the tetrahedral site to return to the octahedral site of the transition metal layer and thus minimize the initial voltage hysteresis and voltage fading on long-term cycling.[158] Similar to crystal structure tuning, careful compositional control has resulted in suppression of voltage fading in Li-rich materials. For example, Kang and coworkers showed that increasing the Ni content from 20% to 40% in $Li_{1.2}Ni_xMn_{0.8-x}O_2$ can improve the voltage stability.[159] The underlying mechanism is the introduction of Ni^{3+} species with increasing Ni content in the material. Irreversible oxygen redox necessitates the triggering of another redox couple in the form of Mn^{3+}/Mn^{4+} in Li/Mn-rich

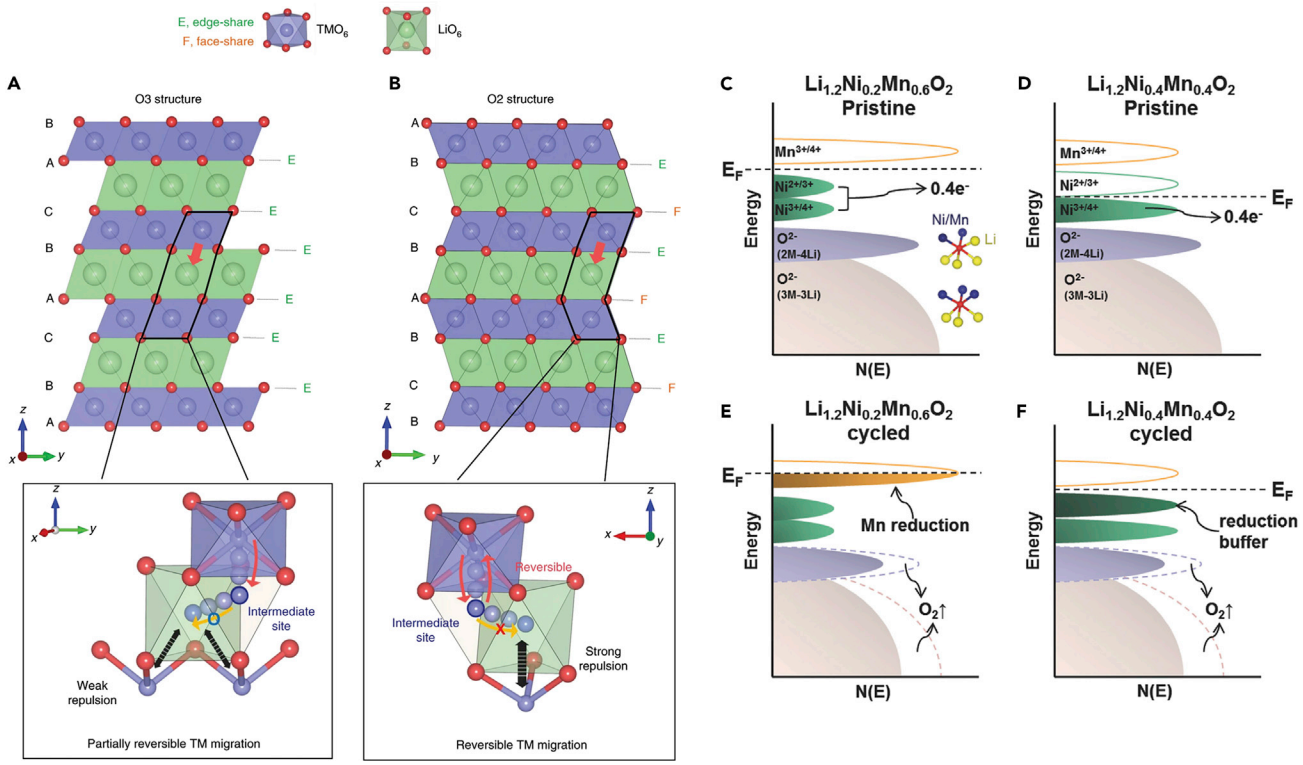

Figure 19. Suppressing Voltage Fading through Tuning the Crystal Structure and the Composition of Li-Rich Cathodes

(A) Crystal structure of an O3-type layered oxide (top). A schematic representation of a transition metal migration pathway in an O3-type layered oxide (bottom). Adapted from Eum et al.[158]

(B) Crystal structure of an O2-type layered oxide (top). A schematic representation of a transition metal migration pathway in an O2-type layered oxide (bottom). Adapted from Eum et al.[158]

(C–F) Schematic electronic band structure of (C) pristine and (E) cycled $Li_{1.2}Ni_{0.2}Mn_{0.6}O_2$, and (D) pristine and (F) cycled $Li_{1/2}Ni_{0.4}Mn_{0.4}O_2$. Adapted from Ku et al.[159]

materials. Formation of Mn^{3+} is detrimental to the voltage stability because Mn^{3+} can migrate to the Li site and form a spinel phase. However, Ni^{3+} is more likely to be reduced than Mn^{4+} in $Li_{1.2}Ni_{0.4}Mn_{0.4}O_2$ because the empty Ni^{2+}/Ni^{3+} states lie below the Mn^{3+}/Mn^{4+} states (Figures 19D and 19F). Hence, the Mn^{3+}/Mn^{4+} redox couple is not triggered for charge compensation (Figures 19E and 19F). Controlling redox couple evolution such as suppressing the activation of Mn^{3+}/Mn^{4+} redox couple in charge compensation can also mitigate voltage fading in Mn-based sodium layered oxide materials.[32] A significant voltage decay in $Na_{0.6}[Li_{0.2}Mn_{0.8}]O_2$ is observed in comparison with $Na_{2/3}[Mg_{1/3}Mn_{2/3}]O_2$ because of the larger contribution of Mn in charge compensation in the former.[32] K^+ doping in $Li_{1.2}Mn_{0.54}Co_{0.13}Ni_{0.13}O_2$ is reported to slow down voltage decay.[157] On K^+ free $Li_{1.2}Mn_{0.54}Co_{0.13}Ni_{0.13}O_2$, the Mn^{4+}/Mn^{3+} redox continuously shifts to lower potential, contributing to voltage decay, along with a continuous growth of the spinel phase. Meanwhile, the K^+ doping is argued to suppress spinel phase formation and the polarization of Mn^{4+}/Mn^{3+} redox coupling, resulting in comparatively lesser voltage decay in the material. Meanwhile, a gradient distribution of Li (Li-poor surface and Li-rich bulk) has been proposed as a strategy to stabilize Li-rich materials.[161] The Li-poor surface is claimed to be immune to irreversible oxygen redox while the bulk can still maintain the high capacity from oxygen redox. Interestingly, Pan and coworkers reported that utilizing a novel non-electroactive cathode component, e.g., sodium carboxymethyl cellulose (CMC) binder, can enhance the cycling performance of

$Li_{1.2}Mn_{0.54}Co_{0.13}Ni_{0.13}O_2$.[162] CMC binder can prevent the detachment of the electroactive particles and also suppress voltage fading of $Li_{1.2}Mn_{0.54}Co_{0.13}Ni_{0.13}O_2$ by Na^+ incorporation from the binder into the cathode particles. The incorporated Na^+ can suppress transition metal migration to the Li site and prevent capacity and voltage fading.

Surface Coating to Prevent Irreversible Oxygen Redox

Various surface coatings are applied to prevent irreversible oxygen redox, such as Li_3PO_4,[163] Zr-based oxides (e.g., Li_2ZrO_3, ZrO_2),[164–167] Co_3O_4,[168] Li_2SiO_3,[169] SnO_2,[170] Al_2O_3,[171–173] and AlF_3.[174] These surface coatings are argued to suppress oxygen release by acting as a barrier between the cathode and the electrolyte, preventing oxygen loss,[175] electrolyte oxidation,[163] transition metal dissolution,[169,170] and structural transformations.[163,165,167] Often these benefits are accompanied by the sacrifice of initial discharge capacity because of the utilization of electrochemically inactive coating materials.[175] Electronic and ionic conductivities are also compromised because of the structural mismatch between the coating and the cathode particle.[176] Hence, phase compatibility becomes an important factor in maintaining the electronic and ionic conductivities of the coated materials.[176] Hu et al. reported a phase-compatible coating of $La_{0.8}Sr_{0.2}MnO_{3-y}$ (LSM) on Li-rich $Li_{1.2}Ni_{0.13}Co_{0.13}Mn_{0.54}O_2$.[176] The LSM coating has a hexagonal crystal structure, and the (012) plane of the coating consists of Mn octahedra with Mn–O bond length of 1.96 Å. The bond length is almost similar to the TM–O bond length of the Li-rich material, allowing a heterostructural connection between the coating and the cathode particle. The authors reported that such phase-compatible coating can mitigate transition metal migration and irreversible oxygen redox, and protect the cathode particle against hydrogen fluoride generation. Zhang et al. reported a dielectric Mg_2TiO_4 coating on $Li_{1.2}Mn_{0.54}Ni_{0.13}Co_{0.13}O_2$, which can create a reverse electric field to inhibit migration of bulk anions to the surface, preventing irreversible oxygen loss.[175] The prevention of oxygen loss resulted in better cycling stability and less voltage fading on the coated material compared with the uncoated one.

Cationic and Anionic Doping/Substitution to Stabilize Oxygen Redox

The incorporation of foreign elements into the crystal lattice can effectively modify the crystal and electronic structure of cathode materials, which can be beneficial for stabilizing oxygen redox. Many different dopants have been studied, and the incorporation of these dopants to a specific lattice site can be carefully controlled. For example, Mg and Zn can be incorporated into the alkali layer and/or the transition metal site simultaneously.[177,178] Meanwhile, elements such as Ti, Nb, Zr, Cr, Al, and Fe are doped into the transition metal site of the layered structure.[179–186] An anionic dopant/substituent such as F can replace some O in the oxide framework of the crystal lattice.[108,187] F can enhance the structural stability by decreasing the Jahn-Teller distortion due to Mn^{3+}.[108] F incorporation into the host lattice has been reported to enhance high-voltage stability of DRX materials.[4] Often, the stability is rationalized based on greater contribution of transition metal cations to redox reactions with respect to the oxygen anions. F substitution can reduce the effective anionic charge, thus lowering the positive charge on the transition metals. Lower positive charge on the transition metals results in larger capacity from the redox activity of the transition metals, which can limit the contribution of oxygen to redox reactions.[113] A strategy of F substitution and high-valence-state transition metal ion incorporation has enabled triggering of the facile redox of Mn^{2+}/Mn^{4+} in Mn-based DRX materials.[113] Thus, high capacity can be obtained without triggering extensive oxygen redox. Consequently, the degradation of cathode materials related to irreversible oxygen redox can be minimized. However, the effect of F

doping/substitution can extend beyond to modifying the electronic structure of transition metal cations and oxygen anions. For example, unlike the oxide version of the DRX material, simultaneous redox of Mn and O can be observed in $Li_2Mn_{2/3}Nb_{1/3}O_2F$ because of the overlap between Mn e_g* states and unhybridized O 2p orbitals. The overlap can take place because of the Mn–F bonds and longer separation between Mn and the anions.[113] Meanwhile, cationic dopants such as Ti^{4+} can stabilize the oxygen environment by strengthening the bonding between metal and oxygen.[10,188,189] Mg^{2+} is reported to act as a pillar when sitting in the alkali layer, thus stabilizing the structure at high SOCs.[178] Mg^{2+} can also improve the electrochemical stability by breaking the alkali-ion/vacancy ordering.[10] Zn^{2+} doping can reduce Mn^{3+}-induced Jahn-Teller distortion and can enhance phase stability.[177] Intentional incorporation of proton in the Li layer of the Li-rich oxides is reported to improve the initial Coulombic efficiency and discharge capacity.[190] Protons can be incorporated in the host structure through solution treatment of the pristine material at different pH.[190] A moderate coupling between the oxidized lattice oxygen and the inserted proton is observed, which is claimed to improve the stability of the oxygen redox activity.

Some dopants such as Ti,[10,188] Zr,[185] and W[191] are observed to segregate preferentially on the surface of the cathode particles. The segregation on the surface can form a protective layer between the cathode and the electrolyte, similar to the coating on a cathode particle. For example, Ti when segregated to the surface of the cathode particle can stabilize the interface because of the strong Ti–O bonding, and minimize the interfacial degradation phenomena.[10,188] Doping with multiple elements with unique distribution from the surface to the bulk can enhance the surface-to-bulk structural and chemical stability of conventional Li layered cathodes,[192] and the strategy can be adapted for stabilization of Li-rich layered oxides as well.[148,183] Shin et al. conducted a comprehensive study of many dopants to theoretically ascertain the tendency of the dopants to segregate on the surface of the particle.[97] The authors calculated the dopant segregation energy at the low index surface facets (namely two surface facets (001) and (010), and three subsurface facets (100), (110), and (111)) of Li_2MnO_3, which is summarized in Figure 20. The study effectively summarized the segregation behavior of the dopants and provided a reference point for identifying dopants to impart surface stability on the Li-rich cathodes. These calculations are based on thermodynamics. During the practical synthesis, kinetic parameters, such as temperature profile, will likely govern how dopants redistribute in cathode particles.[193]

CONCLUSIONS AND PERSPECTIVE

Oxygen redox chemistry in alkali-ion batteries has opened up new opportunities for designing materials with high capacity and energy density. The large capacity obtained by the Li-rich materials has intrigued battery scientists in figuring out the chemistry behind the excess capacity. Early explanations included irreversible structural transformations and Li and O extraction.[11,14] However, from various pioneering works,[15,16,26,37,43,62,63,117,194] it is now widely accepted that the excess capacity can be obtained by the reversible redox chemistry of lattice oxygen. In conventional layered oxides, holes created by electron removal at a deeper delithiation/desodiation level can be trapped at the O 2p orbitals, causing oxygen redox.[25] This type of oxygen redox is often deemed irreversible. However, recent studies on the reversible nature of high-voltage lattice oxygen redox in conventional layered oxides warrants further investigation.[24,33] Li-O-Li configurations have been identified as critical structural units for triggering reversible oxygen redox in Li-rich materials.[15] However, the true nature of oxidized

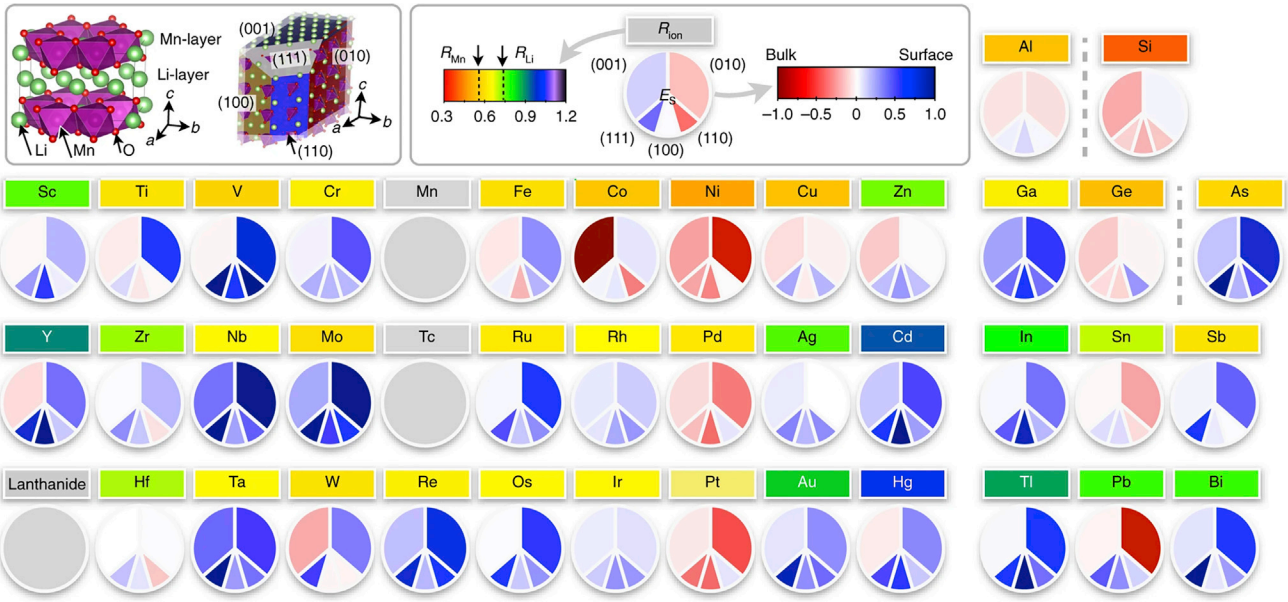

Figure 20. Segregation Behavior of Dopants Calculated in Terms of Dopant Segregation Energy at Various Low Index Surface Facets of Li_2MnO_3
The background rainbow color scheme of the element labeling indicates the radius of the elements. The segregation preference of the dopants is represented by a pie chart, and each segment of the pie chart belongs to a different facet. The segments are colored differently based on the segregation behavior of a dopant, with blue color indicating that the dopant would tend to segregate on the surface of that facet while the red color means that the dopant would prefer to stay in the bulk. Adapted from Shin et al.[97]

oxygen is still under debate. Some studies indicate localized holes in the O 2p orbitals,[43] whereas others claim significant structural transformations with the formation of peroxo-like bonding along with ligand (oxidized oxygen) to transition metal ion charge transfer.[26,28] Recently, molecular oxygen entrapment in the lattice has also been presented as a possible model of lattice oxygen redox.[41] In this review, we have summarized these models of oxygen redox to develop a convenient understanding for readers. While many techniques such as XPS,[44–46] DEMS,[195–197] and electron paramagnetic resonance[63] are utilized to probe the chemical nature of oxygen redox, the recent development of RIXS has unequivocally proved the reversible nature of the lattice oxygen redox.[51,143] Through resolving the emission energy against the excitation energy of the fluorescence photons, the true signature of oxidized oxygen has been resolved. Such resolution has also enabled deciphering of the chemical nature of the oxidized lattice oxygen and has provided critical information on the bulk process of the lattice oxygen redox.[28,42] However, we note that the theoretical interpretation of the RIXS results of the transition metal oxide-based system remains elusive, although it may provide the most direct modeling related to the fundamental mechanism of oxygen redox reactions. We are aware of the current debate over the most legitimate analytical tools to probe the oxygen redox chemistry. We believe that a complete understanding of the highly controversial anionic redox requires a comprehensive diagnostic toolbox that can probe oxygen redox chemistry at multiple length and time scales.

We have also summarized the challenges with oxygen redox that prohibit the commercialization of the Li-rich cathode materials. Transition metal migration to the alkali metal-ion layer is widely observed in materials with oxygen redox.[117] Such migration has contributed to voltage fading on consecutive cycling. This migration is often accompanied by oxygen evolution and structural transformations.[30] The loss of oxygen induces the reduction of some transition metals, which can form new redox couples during subsequent cycling. The evolution of Mn- and Co-based redox

couples has been found to contribute to the voltage fading of Li- and Mn-rich cathode materials.[30] Transition metal migration can alter the electronic structure of cathode material and change the redox sequence, causing redox asymmetry (cationic-to-anionic oxidation on charge and cationic-to-anionic reduction on discharge).[28] Voltage hysteresis and fading have also been reported to originate from such asymmetric redox evolution. A recent study of oxygen redox in $Na_{2/3}Ni_{1/3}Mn_{2/3}O_2$ raises further questions regarding the mechanistic understanding of voltage hysteresis and oxygen redox.[23] This material can utilize oxygen redox for charge compensation but with very little voltage hysteresis (<0.1 V), i.e., almost perfect electrochemical kinetics. No doubt a complicated relationship exists between oxygen redox, transition metal migration, transition metal reduction, and voltage hysteresis and fading. Further development of oxygen redox chemistry will involve the formulation of a unified understanding of oxygen redox to that of transition metal migration and voltage fading. Meanwhile, the critical challenges inhibiting the practical application of oxygen redox, such as voltage hysteresis, voltage fading, and slow oxygen redox kinetics, call for materials development that can address these issues. Future development of cathode materials with oxygen redox may focus on engineering the crystal structure and exploring the compositional space in order to tackle these issues. Enhancing the reversibility of transition metal migration can be promoted by tuning the crystal structure (e.g., O2-type structure over O3-type structure) that can suppress voltage fading on electrochemical cycling.[158] Controlling the long-range ordering of transition metals also provides a means of reducing voltage hysteresis.[41] Meanwhile, close composition control of transition metals can suppress irreversible oxygen evolution.[159] Exploring the compositional space also provides an opportunity for improving oxygen redox kinetics. For example, incorporating Co in $Na_{0.6}[Mg_{0.2}Mn_{0.8-x}Co_x]O_2$ can reduce the band-gap energy and enable facile electron transfer from Co 3d and O 2p states. This results in improved rate capability of the material.[198]

Oxygen redox allows the development of high-energy cathode materials as an alternative to Li-ion cathodes. Sodium layered cathodes constitute such examples. In this review we have summarized that oxygen redox can be triggered in sodium layered cathodes, which can improve the capacity and energy density.[94,179] Crystal structures of sodium layered cathodes are more diverse than those of Li counterparts, and the compositional space is also vastly expanded.[83] Thus, along with utilizing oxygen redox, sodium layered cathodes can be synthesized with cheap and abundant transition metals, improving the cost-effectiveness of these materials.[199] Moreover, the broad range of crystal structures can provide an opportunity to minimize transition metal migration, thus suppressing voltage fading.

ACKNOWLEDGMENTS

The work was supported by the National Science Foundation under contracts DMR 1832613 and CBET 1912885, as well as Virginia Tech College of Science Dean's Discovery Fund. The disordered rocksalt effort was supported by The Thomas F. and Kate Miller Jeffress Memorial Trust, Bank of America, Trustee and the Jeffress Trust Awards Program in Interdisciplinary Research. The authors acknowledge Dr. Wanli Yang for valuable discussion.

AUTHOR CONTRIBUTIONS

Conceptualization, M.M.R. and F.L.; Visualization, M.M.R.; Writing – Original Draft, M.M.R.; Writing – Review and Editing, M.M.R. and F.L.; Funding Acquisition, F.L.; Supervision, F.L.

REFERENCES

1. Li, M., Liu, T., Bi, X., Chen, Z., Amine, K., Zhong, C., and Lu, J. (2020). Cationic and anionic redox in lithium-ion based batteries. Chem. Soc. Rev. *49*, 1688–1705.
2. Assat, G., and Tarascon, J.M. (2018). Fundamental understanding and practical challenges of anionic redox activity in Li-ion batteries. Nat. Energy *3*, 373–386.
3. Grimaud, A., Hong, W.T., Shao-Horn, Y., and Tarascon, J.-M. (2016). Anionic redox processes for electrochemical devices. Nat. Mater. *15*, 121–126.
4. Clément, R.J., Lun, Z., and Ceder, G. (2020). Cation-disordered rocksalt transition metal oxides and oxyfluorides for high energy lithium-ion cathodes. Energy Environ. Sci. *13*, 345–373.
5. Ozawa, K. (1994). Lithium-ion rechargeable batteries with $LiCoO_2$ and carbon electrodes: the $LiCoO_2$/C system. Solid State Ionics *69*, 212–221.
6. Ohzuku, T., and Makimura, Y. (2001). Layered lithium insertion material of $LiCo_{1/3}Ni_{1/3}Mn_{1/3}O_2$ for lithium-ion batteries. Chem. Lett. *30*, 642–643.
7. Lyu, P., Huo, Y., Qu, Z., and Rao, Z. (2020). Investigation on the thermal behavior of Ni-rich NMC lithium ion battery for energy storage. Appl. Therm. Eng. *166*, 114749.
8. Wood, M., Li, J., Ruther, R.E., Du, Z., Self, E.C., Meyer, H.M., III, Daniel, C., Belharouak, I., and Wood, D.L. (2020). Chemical stability and long-term cell performance of low-cobalt, Ni-rich cathodes prepared by aqueous processing for high-energy Li-Ion batteries. Energy Storage Mater. *24*, 188–197.
9. Mu, L., Kan, W.H., Kuai, C., Yang, Z., Li, L., Sun, C.J., Sainio, S., Avdeev, M., Nordlund, D., and Lin, F. (2020). Structural and electrochemical impacts of Mg/Mn dual dopants on the $LiNiO_2$ cathode in Li-metal batteries. ACS Appl. Mater. Interfaces *12*, 12874–12882.
10. Mu, L., Zhang, R., Kan, W.H., Zhang, Y., Li, L., Kuai, C., Zydlewski, B., Rahman, M.M., Sun, C.-J., Sainio, S., et al. (2019). Dopant distribution in Co-free high-energy layered cathode materials. Chem. Mater. *31*, 9769–9776.
11. Lu, Z., and Dahn, J.R. (2002). Understanding the anomalous capacity of $Li/Li[Ni_xLi_{(1/3-2x/3)}Mn_{(2/3-x/3)}]O_2$ cells using in situ X-ray diffraction and electrochemical studies. J. Electrochem. Soc. *149*, A815.
12. Lu, Z., Beaulieu, L.Y., Donaberger, R.A., Thomas, C.L., and Dahn, J.R. (2002). Synthesis, structure, and electrochemical behavior of $LiNi_xLi_{1/3-2x/3}Mn_{2/3-x/3}O_2$. J. Electrochem. Soc. *149*, A778.
13. Lu, Z., Chen, Z., and Dahn, J.R. (2003). Lack of cation clustering in $Li[Ni_xLi_{1/3-2x/3}Mn_{2/3-x/3}]O_2$ ($0 < x \leq 1/2$) and $Li[Cr_xLi_{(1-x)/3}Mn_{(2-2x)/3}]O_2$ ($0 < x < 1$). Chem. Mater. *15*, 3214–3220.
14. Thackeray, M.M., Kang, S.H., Johnson, C.S., Vaughey, J.T., Benedek, R., and Hackney, S.A. (2007). Li_2MnO_3-stabilized $LiMO_2$ (M = Mn, Ni, Co) electrodes for lithium-ion batteries. J. Mater. Chem. *17*, 3112–3125.
15. Seo, D.-H., Lee, J., Urban, A., Malik, R., Kang, S., and Ceder, G. (2016). The structural and chemical origin of the oxygen redox activity in layered and cation-disordered Li-excess cathode materials. Nat. Chem. *8*, 692–697.
16. Luo, K., Roberts, M.R., Hao, R., Guerrini, N., Pickup, D.M., Liu, Y.S., Edström, K., Guo, J., Chadwick, A.V., Duda, L.C., et al. (2016). Charge-compensation in 3d-transition-metal-oxide intercalation cathodes through the generation of localized electron holes on oxygen. Nat. Chem. *8*, 684–691.
17. Wang, R., Li, X., Liu, L., Lee, J., Seo, D.H., Bo, S.H., Urban, A., and Ceder, G. (2015). A disordered rock-salt Li-excess cathode material with high capacity and substantial oxygen redox activity: $Li_{1.25}Nb_{0.25}Mn_{0.5}O_2$. Electrochem. Commun. *60*, 70–73.
18. Li, B., Shao, R., Yan, H., An, L., Zhang, B., Wei, H., Ma, J., Xia, D., and Han, X. (2016). Understanding the stability for Li-rich layered oxide Li_2RuO_3 cathode. Adv. Funct. Mater. *26*, 1330–1337.
19. Lee, J., Urban, A., Li, X., Su, D., Hautier, G., and Ceder, G. (2014). Unlocking the potential of cation-disordered oxides for rechargeable lithium batteries. Science *343*, 519–522.
20. Yabuuchi, N., Takeuchi, M., Nakayama, M., Shiiba, H., Ogawa, M., Nakayama, K., Ohta, T., Endo, D., Ozaki, T., Inamasu, T., et al. (2015). High-capacity electrode materials for rechargeable lithium batteries: Li_3NbO_4-based system with cation-disordered rocksalt structure. Proc. Natl. Acad. Sci. U S A *112*, 7650–7655.
21. Lun, Z., Ouyang, B., Cai, Z., Clément, R.J., Kwon, D.H., Huang, J., Papp, J.K., Balasubramanian, M., Tian, Y., McCloskey, B.D., et al. (2020). Design principles for high-capacity Mn-based cation-disordered rocksalt cathodes. Chem *6*, 153–168.
22. Kitchaev, D.A., Lun, Z., Richards, W.D., Ji, H., Clément, R.J., Balasubramanian, M., Kwon, D.H., Dai, K., Papp, J.K., Lei, T., et al. (2018). Design principles for high transition metal capacity in disordered rocksalt Li-ion cathodes. Energy Environ. Sci. *11*, 2159–2171.
23. Dai, K., Mao, J., Zhuo, Z., Feng, Y., Mao, W., Ai, G., Pan, F., Chuang, Y., Liu, G., and Yang, W. (2020). Negligible voltage hysteresis with strong anionic redox in conventional battery electrode. Nano Energy *74*, 104831.
24. Lee, G.-H., Wu, J., Kim, D., Cho, K., Cho, M., Yang, W., and Kang, Y.-M. (2020). Reversible anionic redox activities in conventional $LiNi_{1/3}Co_{1/3}Mn_{1/3}O_2$ cathodes. Angew. Chem. Int. Ed. *59*, 8681–8688.
25. Goodenough, J.B., and Park, K.S. (2013). The Li-ion rechargeable battery: a perspective. J. Am. Chem. Soc. *135*, 1167–1176.
26. Ben Yahia, M., Vergnet, J., Saubanère, M., and Doublet, M.L. (2019). Unified picture of anionic redox in Li/Na-ion batteries. Nat. Mater. *18*, 496–502.
27. McCalla, E., Abakumov, A.M., Saubanère, M., Foix, D., Berg, E.J., Rousse, G., Doublet, M.L., Gonbeau, D., Novák, P., Van Tendeloo, G., et al. (2015). Visualization of O-O peroxo-like dimers in high-capacity layered oxides for Li-ion batteries. Science *350*, 1516–1521.
28. Gent, W.E., Lim, K., Liang, Y., Li, Q., Barnes, T., Ahn, S.-J., Stone, K.H., McIntire, M., Hong, J., Song, J.H., et al. (2017). Coupling between oxygen redox and cation migration explains unusual electrochemistry in lithium-rich layered oxides. Nat. Commun. *8*, 2091.
29. Assat, G., Foix, D., Delacourt, C., Iadecola, A., Dedryvère, R., and Tarascon, J.M. (2017). Fundamental interplay between anionic/cationic redox governing the kinetics and thermodynamics of lithium-rich cathodes. Nat. Commun. *8*, 2219.
30. Hu, E., Yu, X., Lin, R., Bi, X., Lu, J., Bak, S., Nam, K.W., Xin, H.L., Jaye, C., Fischer, D.A., et al. (2018). Evolution of redox couples in Li- and Mn-rich cathode materials and mitigation of voltage fade by reducing oxygen release. Nat. Energy *3*, 690–698.
31. Li, N., Hwang, S., Sun, M., Fu, Y., Battaglia, V.S., Su, D., and Tong, W. (2019). Unraveling the voltage decay phenomenon in Li-rich layered oxide cathode of no oxygen activity. Adv. Energy Mater. *9*, 1902258.
32. Wu, J., Zhuo, Z., Rong, X., Dai, K., Lebens-Higgins, Z., Sallis, S., Pan, F., Piper, L.F.J., Liu, G., Chuang, Y., et al. (2020). Dissociate lattice oxygen redox reactions from capacity and voltage drops of battery electrodes. Sci. Adv. *6*, eaaw3871.
33. Li, N., Sallis, S., Papp, J.K., Wei, J., McCloskey, B.D., Yang, W., and Tong, W. (2019). Unraveling the cationic and anionic redox reactions in a conventional layered oxide cathode. ACS Energy Lett. *4*, 2836–2842.
34. Zaanen, J., Sawatzky, G.A., and Allen, J.W. (1985). Band gaps and electronic structure of transition-metal compounds. Phys. Rev. Lett. *55*, 418–421.
35. Saubanère, M., McCalla, E., Tarascon, J.-M., and Doublet, M.-L. (2016). The intriguing question of anionic redox in high-energy density cathodes for Li-ion batteries. Energy Environ. Sci. *9*, 984–991.
36. Li, X., Qiao, Y., Guo, S., Xu, Z., Zhu, H., Zhang, X., Yuan, Y., He, P., Ishida, M., and Zhou, H. (2018). Direct visualization of the reversible O^{2-}/O^{-} redox process in Li-rich cathode materials. Adv. Mater. *30*, 1705197.
37. Sathiya, M., Rousse, G., Ramesha, K., Laisa, C.P., Vezin, H., Sougrati, M.T., Doublet, M.-L., Foix, D., Gonbeau, D., Walker, W., et al. (2013). Reversible anionic redox chemistry in high-capacity layered-oxide electrodes. Nat. Mater. *12*, 827–835.
38. Lebens-Higgins, Z.W., Chung, H., Zuba, M.J., Rana, J., Li, Y., Faenza, N.V., Pereira, N., McCloskey, B.D., Rodolakis, F., Yang, W., et al. (2020). How bulk sensitive is hard X-ray photoelectron spectroscopy: accounting for the cathode-electrolyte interface when addressing oxygen redox. J. Phys. Chem. Lett. *11*, 2106–2112.
39. Hong, J., Gent, W.E., Xiao, P., Lim, K., Seo, D.-H., Wu, J., Csernica, P.M., Takacs, C.J.,

Nordlund, D., Sun, C.-J., et al. (2019). Metal-oxygen decoordination stabilizes anion redox in Li-rich oxides. Nat. Mater. *18*, 256–265.

40. House, R.A., Rees, G.J., Pérez-Osorio, M.A., Marie, J.-J., Boivin, E., Robertson, A.W., Nag, A., Garcia-Fernandez, M., Zhou, K.-J., and Bruce, P.G. (2020). First-cycle voltage hysteresis in Li-rich 3d cathodes associated with molecular O_2 trapped in the bulk. Nat. Energy *5*, 777–785.

41. House, R.A., Maitra, U., Pérez-Osorio, M.A., Lozano, J.G., Jin, L., Somerville, J.W., Duda, L.C., Nag, A., Walters, A., Zhou, K.-J., et al. (2020). Superstructure control of first-cycle voltage hysteresis in oxygen-redox cathodes. Nature *577*, 502–508.

42. Zhuo, Z., Liu, Y., Guo, J., Chuang, Y., Pan, F., and Yang, W. (2020). Full energy range resonant inelastic X-ray scattering of O_2 and CO_2: direct comparison with oxygen redox state in batteries. J. Phys. Chem. Lett. *11*, 2618–2623.

43. Maitra, U., House, R.A., Somerville, J.W., Tapia-Ruiz, N., Lozano, J.G., Guerrini, N., Hao, R., Luo, K., Jin, L., Pérez-Osorio, M.A., et al. (2018). Oxygen redox chemistry without excess alkali-metal ions in $Na_{2/3}[Mg_{0.28}Mn_{0.72}]O_2$. Nat. Chem. *10*, 288–295.

44. Carroll, K.J., Qian, D., Fell, C., Calvin, S., Veith, G.M., Chi, M., Baggetto, L., and Meng, Y.S. (2013). Probing the electrode/electrolyte interface in the lithium excess layered oxide $Li_{1.2}Ni_{0.2}Mn_{0.6}O_2$. Phys. Chem. Chem. Phys. *15*, 11128–11138.

45. Assat, G., Iadecola, A., Foix, D., Dedryvere, R., and Tarascon, J.-M. (2018). Direct quantification of anionic redox over long cycling of Li-rich NMC via hard X-ray photoemission spectroscopy. ACS Energy Lett. *3*, 2721–2728.

46. Foix, D., Sathiya, M., McCalla, E., Tarascon, J.-M., and Gonbeau, D. (2016). X-ray photoemission spectroscopy study of cationic and anionic redox processes in high-capacity Li-ion battery layered-oxide electrodes. J. Phys. Chem. C *120*, 862–874.

47. Yang, W., and Devereaux, T.P. (2018). Anionic and cationic redox and interfaces in batteries: advances from soft X-ray absorption spectroscopy to resonant inelastic scattering. J. Power Sources *389*, 188–197.

48. Roychoudhury, S., Qiao, R., Zhuo, Z., Li, Q., Lyu, Y., Kim, J., Liu, J., Lee, E., Polzin, B.J., Guo, J., et al. (2020). Deciphering the oxygen absorption pre-edge: a caveat on its application for probing oxygen redox reactions in batteries. Energy Environ. Mater. https://doi.org/10.1002/eem2.12119.

49. House, R.A., Maitra, U., Jin, L., Lozano, J.G., Somerville, J.W., Rees, N.H., Naylor, A.J., Duda, L.C., Massel, F., Chadwick, A.V., et al. (2019). What triggers oxygen loss in oxygen redox cathode materials? Chem. Mater. *31*, 3293–3300.

50. Dai, K., Wu, J., Zhuo, Z., Li, Q., Sallis, S., Mao, J., Ai, G., Sun, C., Li, Z., Gent, W.E., et al. (2019). High reversibility of lattice oxygen redox quantified by direct bulk probes of both anionic and cationic redox reactions. Joule *3*, 518–541.

51. Zhuo, Z., Pemmaraju, C.D., Vinson, J., Jia, C., Moritz, B., Lee, I., Sallies, S., Li, Q., Wu, J., Dai, K., et al. (2018). Spectroscopic signature of oxidized oxygen states in peroxides. J. Phys. Chem. Lett. *9*, 6378–6384.

52. Rong, X., Liu, J., Hu, E., Liu, Y., Wang, Y., Wu, J., Yu, X., Page, K., Hu, Y.-S., Yang, W., et al. (2018). Structure-induced reversible anionic redox activity in Na layered oxide cathode. Joule *2*, 125–140.

53. Bréger, J., Dupré, N., Chupas, P.J., Lee, P.L., Proffen, T., Parise, J.B., and Grey, C.P. (2005). Short- and long-range order in the positive electrode material, $Li(NiMn)_{0.5}O_2$: a joint X-ray and neutron diffraction, pair distribution function analysis and NMR study. J. Am. Chem. Soc. *127*, 7529–7537.

54. Lim, J.-H., Bang, H., Lee, K.-S., Amine, K., and Sun, Y.-K. (2009). Electrochemical characterization of Li_2MnO_3-$Li[Ni_{1/3}Co_{1/3}Mn_{1/3}]O_2$-$LiNiO_2$ cathode synthesized via co-precipitation for lithium secondary batteries. J. Power Sources *189*, 571–575.

55. Zhao, T., Chen, S., Li, L., Zhang, X., Chen, R., Belharouak, I., Wu, F., and Amine, K. (2013). Synthesis, characterization, and electrochemistry of cathode material $Li[Li_{0.2}Co_{0.13}Ni_{0.13}Mn_{0.54}]O_2$ using organic chelating agents for lithium-ion batteries. J. Power Sources *228*, 206–213.

56. Zhou, F., Zhao, X., van Bommel, A., Xia, X., and Dahn, J.R. (2011). Comparison of $Li[Li_{1/9}Ni_{1/9}]Mn_{5/9}O_2$, $Li[Li_{1/5}Ni_{1/5}Mn_{3/5}]O_2$, $Li[Ni_{0.5}Mn_{1.5}]O_4$, and $Li[Ni_{2/3}Mn_{1/9}]O_2$ as high voltage positive electrode materials. J. Electrochem. Soc. *158*, A187.

57. Barkhouse, D.A.R., and Dahn, J.R. (2005). A novel fabrication technique for producing dense $Li[Ni_xLi_{(1/3-2x/3)}Mn_{(2/3-x/3)}]O_2$, $0 \le x \le 1/2$. J. Electrochem. Soc. *152*, A746.

58. Kang, S.-H., Johnson, C.S., Vaughey, J.T., Amine, K., and Thackeray, M.M. (2006). The effects of acid treatment on the electrochemical properties of $0.5Li_2MnO_3 \cdot 0.5LiNi_{0.44}Co_{0.25}Mn_{0.31}O_2$ electrodes in lithium cells. J. Electrochem. Soc. *153*, A1186.

59. Sun, Y.-K., Kim, M.G., Kang, S.-H., and Amine, K. (2003). Electrochemical performance of layered $Li[Li_{0.15}Ni_{0.275-x}Mg_xMn_{0.575}]O_2$ cathode materials for lithium secondary batteries. J. Mater. Chem. *13*, 319–322.

60. Kang, S.-H., Sun, Y.-K., and Amine, K. (2003). Electrochemical and ex situ X-ray study of $Li(Li_{0.2}Ni_{0.2}Mn_{0.6})O_2$ cathode material for Li secondary batteries. Electrochem. Solid State Lett. *6*, A183.

61. Chen, Z., Sun, Y.-K., and Amine, K. (2006). Electrochemical properties of lithium-rich $Li_{1+x}(Mn_{1/9}Ni_{1/9}Co_{1/9})_{1-x}O_2$ at high potential. J. Electrochem. Soc. *153*, A1818.

62. Koga, H., Croguennec, L., Ménétrier, M., Mannessiez, P., Weill, F., and Delmas, C. (2013). Different oxygen redox participation for bulk and surface: a possible global explanation for the cycling mechanism of $Li_{1.20}Mn_{0.54}Co_{0.13}Ni_{0.13}O_2$. J. Power Sources *236*, 250–258.

63. Koga, H., Croguennec, L., Ménétrier, M., Douhil, K., Belin, S., Bourgeois, L., Suard, E., Weill, F., and Delmas, C. (2013). Reversible oxygen participation to the redox processes revealed for $Li_{1.20}Mn_{0.54}Co_{0.13}Ni_{0.13}O_2$. J. Electrochem. Soc. *160*, A786–A792.

64. Luo, K., Roberts, M.R., Guerrini, N., Tapia-Ruiz, N., Hao, R., Massel, F., Pickup, D.M., Ramos, S., Liu, Y.-S., Guo, J., et al. (2016). Anion redox chemistry in the cobalt free 3d transition metal oxide intercalation electrode $Li[Li_{0.2}Ni_{0.2}Mn_{0.6}]O_2$. J. Am. Chem. Soc. *138*, 11211–11218.

65. Assat, G., Delacourt, C., Corte, D.A.D., and Tarascon, J.-M. (2016). Editors' choice—practical assessment of anionic redox in Li-rich layered oxide cathodes: a mixed blessing for high energy Li-ion batteries. J. Electrochem. Soc. *163*, A2965–A2976.

66. Rozier, P., Sathiya, M., Paulraj, A.R., Foix, D., Desaunay, T., Taberna, P.-L., Simon, P., and Tarascon, J.-M. (2015). Anionic redox chemistry in Na-rich $Na_2Ru_{1-y}Sn_yO_3$ positive electrode material for Na-ion batteries. Electrochem. Commun. *53*, 29–32.

67. Tamaru, M., Wang, X., Okubo, M., and Yamada, A. (2013). Layered Na_2RuO_3 as a cathode material for Na-ion batteries. Electrochem. Commun. *33*, 23–26.

68. Perez, A.J., Batuk, D., Saubanère, M., Rousse, G., Foix, D., McCalla, E., Berg, E.J., Dugas, R., Van Den Bos, K.H.W., Doublet, M.-L., et al. (2016). Strong oxygen participation in the redox governing the structural and electrochemical properties of Na-rich layered oxide Na_2IrO_3. Chem. Mater. *28*, 8278–8288.

69. Pearce, P.E., Rousse, G., Karakulina, O.M., Hadermann, J., Van Tendeloo, G., Foix, D., Fauth, F., Abakumov, A.M., and Tarascon, J.-M. (2018). β-$Na_{1.7}IrO_3$: a tridimensional Na-ion insertion material with a redox active oxygen network. Chem. Mater. *30*, 3285–3293.

70. Koga, H., Croguennec, L., Mannessiez, P., Ménétrier, M., Weill, F., Bourgeois, L., Duttine, M., Suard, E., and Delmas, C. (2012). $Li_{1.20}Mn_{0.54}Co_{0.13}Ni_{0.13}O_2$ with different particle sizes as attractive positive electrode materials for lithium-ion batteries: insights into their structure. J. Phys. Chem. C *116*, 13497–13506.

71. Shukla, A.K., Ramasse, Q.M., Ophus, C., Duncan, H., Hage, F., and Chen, G. (2015). Unravelling structural ambiguities in lithium- and manganese-rich transition metal oxides. Nat. Commun. *6*, 8711.

72. Mohanty, D., Huq, A., Payzant, E.A., Sefat, A.S., Li, J., Abraham, D.P., Wood, D.L., and Daniel, C. (2013). Neutron diffraction and magnetic susceptibility studies on a high-voltage $Li_{1.2}Mn_{0.55}Ni_{0.15}Co_{0.10}O_2$ lithium ion battery cathode: insight into the crystal structure. Chem. Mater. *25*, 4064–4070.

73. Yu, H., Ishikawa, R., So, Y.-G., Shibata, N., Kudo, T., Zhou, H., and Ikuhara, Y. (2013). Direct atomic-resolution observation of two phases in the $Li_{1.2}Mn_{0.567}Ni_{0.166}Co_{0.067}O_2$ cathode material for lithium-ion batteries. Angew. Chem. Int. Ed. *52*, 5969–5973.

74. Bréger, J., Jiang, M., Dupré, N., Meng, Y.S., Shao-Horn, Y., Ceder, G., and Grey, C.P. (2005). High-resolution X-ray diffraction,

DIFFaX, NMR and first principles study of disorder in the Li_2MnO_3-$Li[Ni_{1/2}Mn_{1/2}]O_2$ solid solution. J. Solid State Chem. *178*, 2575–2585.

75. Johnson, C.S., Li, N., Vaughey, J.T., Hackney, S.A., and Thackeray, M.M. (2005). Lithium-manganese oxide electrodes with layered-spinel composite structures $xLi_2MnO_3\bullet(1-x)Li_{1+y}Mn_{2-y}O_4$ ($0 < x < 1$, $0 \leq y \leq 0.33$) for lithium batteries. Electrochem. Commun. *7*, 528–536.

76. Rosolen, J.M., and Abbate, M. (2001). XANES and EXAFS of chemically deintercalated $LiCo_{0.5}Ni_{0.5}O_2$. Solid State Ionics *139*, 83–88.

77. Montoro, L.A., Abbate, M., and Rosolen, J.M. (2000). Electronic structure of transition metal ions in deintercalated and reintercalated $LiCo_{0.5}Ni_{0.5}O_2$. J. Electrochem. Soc. *147*, 1651.

78. Yoon, W.S., Kim, K.-B., Kim, M.-G., Lee, M.-K., Shin, H.-J., Lee, J.-M., Lee, J.-S., and Yo, C.-H. (2002). Oxygen contribution on Li-ion intercalation-deintercalation in $LiCoO_2$ investigated by O K-edge and Co L-edge X-ray absorption spectroscopy. J. Phys. Chem. B *106*, 2526–2532.

79. Ma, C., Alvarado, J., Xu, J., Clément, R.J., Kodur, M., Tong, W., Grey, C.P., and Meng, Y.S. (2017). Exploring oxygen activity in the high energy P2-type $Na_{0.78}Ni_{0.23}Mn_{0.69}O_2$ cathode material for Na-ion batteries. J. Am. Chem. Soc. *139*, 4835–4845.

80. Ohzuku, T., Ueda, A., and Nagayama, M. (1993). Electrochemistry and structural chemistry of $LiNiO_2$ (R3m) for 4 volt secondary lithium cells. J. Electrochem. Soc. *140*, 1862.

81. Yoon, W.-S., Chung, K.Y., McBreen, J., Fischer, D.A., and Yang, X.-Q. (2006). Changes in electronic structure of the electrochemically Li-ion deintercalated $LiNiO_2$ system investigated by soft X-ray absorption spectroscopy. J. Power Sources *163*, 234–237.

82. Zhang, Y., Wu, M., Ma, J., Wei, G., Ling, Y., Zhang, R., and Huang, Y. (2020). Revisiting the $Na_{2/3}Ni_{1/3}Mn_{2/3}O_2$ cathode: oxygen redox chemistry and oxygen release suppression. ACS Cent. Sci. *6*, 232–240.

83. Yabuuchi, N., Kubota, K., Dahbi, M., and Komaba, S. (2014). Research development on sodium-ion batteries. Chem. Rev. *114*, 11636–11682.

84. Mu, L., Xu, S., Li, Y., Hu, Y.-S., Li, H., Chen, L., and Huang, X. (2015). Prototype sodium-ion batteries using an air-stable and Co/Ni-free O_3-layered metal oxide cathode. Adv. Mater. *27*, 6928–6933.

85. Rahman, M.M., Zhang, Y., Xia, S., Kan, W.H., Avdeev, M., Mu, L., Sokaras, D., Kroll, T., Du, X.-W., Nordlund, D., et al. (2019). Surface characterization of Li-substituted compositionally heterogeneous $NaLi_{0.045}Cu_{0.185}Fe_{0.265}Mn_{0.505}O_2$ sodium-ion cathode. Mater. J. Phys. Chem. C *123*, 11428–11435.

86. Rahman, M.M., Mao, J., Kan, W.H., Sun, C.-J., Li, L., Zhang, Y., Avdeev, M., Du, X.-W., and Lin, F. (2019). An ordered P2/P3 composite layered oxide cathode with long cycle life in sodium-ion batteries. ACS Mater. Lett. *1*, 573–581.

87. Li, X., Guo, S., Qiu, F., Wang, L., Ishida, M., and Zhou, H. (2019). $Na_2Ru_{1-x}Mn_xO_3$ as the cathode for sodium-ion batteries. J. Mater. Chem. A *7*, 4395–4399.

88. Sun, Y., Guo, S., and Zhou, H. (2019). Adverse effects of interlayer-gliding in layered transition-metal oxides on electrochemical sodium-ion storage. Energy Environ. Sci. *12*, 825–840.

89. Yang, L., Li, X., Liu, J., Xiong, S., Ma, X., Liu, P., Bai, J., Xu, W., Tang, Y., Hu, Y.-Y., et al. (2019). Lithium-doping stabilized high-performance $P2\text{-}Na_{0.66}Li_{0.18}Fe_{0.12}Mn_{0.7}O_2$ cathode for sodium ion batteries. J. Am. Chem. Soc. *141*, 6680–6689.

90. Wang, Q.-C., Meng, J.-K., Yue, X.-Y., Qiu, Q.-Q., Song, Y., Wu, X.-J., Fu, Z.-W., Xia, Y.-Y., Shadike, Z., Wu, J., et al. (2019). Tuning P2-structured cathode material by Na-site Mg substitution for Na-ion batteries. J. Am. Chem. Soc. *141*, 840–848.

91. Yabuuchi, N., Hara, R., Kubota, K., Paulsen, J., Kumakura, S., and Komaba, S. (2014). A new electrode material for rechargeable sodium batteries: P2-type $Na_{2/3}[Mg_{0.28}Mn_{0.72}]O_2$ with anomalously high reversible capacity. J. Mater. Chem. A *2*, 16851–16855.

92. Mortemard de Boisse, B., Nishimura, S., Watanabe, E., Lander, L., Tsuchimoto, A., Kikkawa, J., Kobayashi, E., Asakura, D., Okubo, M., and Yamada, A. (2018). Highly reversible oxygen-redox chemistry at 4.1 V in $Na_{4/7-x}[\square_{1/7}Mn_{6/7}]O_2$ ($\square$: Mn vacancy). Adv. Energy Mater. *8*, 1800409.

93. Yabuuchi, N., Hara, R., Kajiyama, M., Kubota, K., Ishigaki, T., Hoshikawa, A., and Komaba, S. (2014). New O2/P2-type Li-excess layered manganese oxides as promising multi-functional electrode materials for rechargeable Li/Na batteries. Adv. Energy Mater. *4*, 1301453.

94. Cao, X., Li, X., Qiao, Y., Jia, M., Qiu, F., He, Y., He, P., and Zhou, H. (2019). Restraining oxygen loss and suppressing structural distortion in a newly Ti-substituted layered oxide $P2\text{-}Na_{0.66}Li_{0.22}Ti_{0.15}Mn_{0.63}O_2$. ACS Energy Lett. *4*, 2409–2417.

95. Rong, X., Hu, E., Lu, Y., Meng, F., Zhao, C., Wang, X., Zhang, Q., Yu, X., Gu, L., Hu, Y.-S., et al. (2019). Anionic redox reaction-induced high-capacity and low-strain cathode with suppressed phase transition. Joule *3*, 503–517.

96. Robertson, A.D., and Bruce, P.G. (2004). Overcapacity of $Li[Ni_xLi_{1/3-2x/3}Mn_{2/3-x/3}]O_2$ electrodes. Electrochem. Solid State Lett. *7*, A294–A298.

97. Shin, Y., Kan, W.H., Aykol, M., Papp, J.K., McCloskey, B.D., Chen, G., and Persson, K.A. (2018). Alleviating oxygen evolution from Li-excess oxide materials through theory-guided surface protection. Nat. Commun. *9*, 4597.

98. Urban, A., Lee, J., and Ceder, G. (2014). The configurational space of rocksalt-type oxides for high-capacity lithium battery electrodes. Adv. Energy Mater. *4*, 1400478.

99. Urban, A., Abdellahi, A., Dacek, S., Artrith, N., and Ceder, G. (2017). Electronic-structure origin of cation disorder in transition-metal oxides. Phys. Rev. Lett. *119*, 176402.

100. Ji, H., Urban, A., Kitchaev, D.A., Kwon, D.H., Artrith, N., Ophus, C., Huang, W., Cai, Z., Shi, T., Kim, J.C., et al. (2019). Hidden structural and chemical order controls lithium transport in cation-disordered oxides for rechargeable batteries. Nat. Commun. *10*, 592.

101. Chen, D., Kan, W.H., and Chen, G. (2019). Understanding performance degradation in cation-disordered rock-salt oxide cathodes. Adv. Energy Mater. *9*, 1901255.

102. Zhao, E., Li, Q., Meng, F., Liu, J., Wang, J., He, L., Jiang, Z., Zhang, Q., Yu, X., Gu, L., et al. (2019). Stabilizing the oxygen lattice and reversible oxygen redox chemistry through structural dimensionality in lithium-rich cathode oxides. Angew. Chem. Int. Ed. *58*, 4323–4327.

103. Luo, M., Zheng, S., Wu, J., Zhou, K., Zuo, W., Feng, M., He, H., Liu, R., Zhu, J., Zhao, G., et al. (2020). Identifying the anionic redox activity in cation-disordered $Li_{1.25}Nb_{0.25}Fe_{0.50}O_2$/C oxide cathodes for Li-ion batteries. J. Mater. Chem. A *8*, 5115–5127.

104. House, R.A., Jin, L., Maitra, U., Tsuruta, K., Somerville, J.W., Förstermann, D.P., Massel, F., Duda, L., Roberts, M.R., and Bruce, P.G. (2018). Lithium manganese oxyfluoride as a new cathode material exhibiting oxygen redox. Energy Environ. Sci. *11*, 926–932.

105. Chen, D., Wu, J., Papp, J.K., McCloskey, B.D., Yang, W., and Chen, G. (2020). Role of redox-inactive transition-metals in the behavior of cation-disordered rocksalt cathodes. Small *16*, 2000656.

106. Freire, M., Kosova, N.V., Jordy, C., Chateigner, D., Lebedev, O.I., Maignan, A., and Pralong, V. (2016). A new active Li-Mn-O compound for high energy density Li-ion batteries. Nat. Mater. *15*, 173–177.

107. Li, X., Qiao, Y., Guo, S., Jiang, K., Ishida, M., and Zhou, H. (2019). A new type of Li-rich rock-salt oxide $Li_2Ni_{1/3}Ru_{2/3}O_3$ with reversible anionic redox chemistry. Adv. Mater. *31*, 1807825.

108. Lun, Z., Ouyang, B., Kitchaev, D.A., Clément, R.J., Papp, J.K., Balasubramanian, M., Tian, Y., Lei, T., Shi, T., McCloskey, B.D., et al. (2019). Improved cycling performance of Li-excess cation-disordered cathode materials upon fluorine substitution. Adv. Energy Mater. *9*, 1802959.

109. Chen, R., Ren, S., Knapp, M., Wang, D., Witter, R., Fichtner, M., and Hahn, H. (2015). Disordered lithium-rich oxyfluoride as a stable host for enhanced Li^+ intercalation storage. Adv. Energy Mater. *5*, 1401814.

110. Zhao, E., He, L., Wang, B., Li, X., Zhang, J., Wu, Y., Chen, J., Zhang, S., Liang, T., Chen, Y., et al. (2019). Structural and mechanistic revelations on high capacity cation-disordered Li-rich oxides for rechargeable Li-ion batteries. Energy Storage Mater. *16*, 354–363.

111. Ji, H., Kitchaev, D.A., Lun, Z., Kim, H., Foley, E., Kwon, D.-H., Tian, Y., Balasubramanian, M., Bianchini, M., Cai, Z., et al. (2019).

Computational investigation and experimental realization of disordered high-capacity Li-ion cathodes based on Ni redox. Chem. Mater. *31*, 2431–2442.

112. Lun, Z., Ouyang, B., Kwon, D.-H., Ha, Y., Foley, E.E., Huang, T.-Y., Cai, Z., Kim, H., Balasubramanian, M., Sun, Y., et al. (2020). Cation-disordered rocksalt-type high-entropy cathodes for Li-ion batteries. Nat. Mater. https://doi.org/10.1038/s41563-020-00816-0.

113. Lee, J., Kitchaev, D.A., Kwon, D.-H., Lee, C.-W., Papp, J.K., Liu, Y.-S., Lun, Z., Clément, R.J., Shi, T., McCloskey, B.D., et al. (2018). Reversible Mn^{2+}/Mn^{4+} double redox in lithium-excess cathode materials. Nature *556*, 185–190.

114. Zhang, K., Li, B., Zuo, Y., Song, J., Shang, H., Ning, F., and Xia, D. (2019). Voltage decay in layered Li-rich Mn-based cathode materials. Electrochem. Energy Rev. *2*, 606–623.

115. Croy, J.R., Balasubramanian, M., Gallagher, K.G., and Burrell, A.K. (2015). Review of the U.S. Department of Energy's "deep dive" effort to understand voltage fade in Li- and Mn-rich cathodes. Acc. Chem. Res. *48*, 2813–2821.

116. Fell, C.R., Qian, D., Carroll, K.J., Chi, M., Jones, J.L., and Meng, Y.S. (2013). Correlation between oxygen vacancy, microstrain, and cation distribution in lithium-excess layered oxides during the first electrochemical cycle. Chem. Mater. *25*, 1621–1629.

117. Sathiya, M., Abakumov, A.M., Foix, D., Rousse, G., Ramesha, K., Saubanère, M., Doublet, M.-L., Vezin, H., Laisa, C.P., Prakash, A.S., et al. (2015). Origin of voltage decay in high-capacity layered oxide electrodes. Nat. Mater. *14*, 230–238.

118. Myeong, S., Cho, W., Jin, W., Hwang, J., Yoon, M., Yoo, Y., Nam, G., Jang, H., Han, J.G., Choi, N.S., et al. (2018). Understanding voltage decay in lithium-excess layered cathode materials through oxygen-centred structural arrangement. Nat. Commun. *9*, 3285.

119. Lin, F., Markus, I.M., Nordlund, D., Weng, T.-C., Asta, M.D., Xin, H.L., and Doeff, M.M. (2014). Surface reconstruction and chemical evolution of stoichiometric layered cathode materials for lithium-ion batteries. Nat. Commun. *5*, 3529.

120. Mu, L., Lin, R., Xu, R., Han, L., Xia, S., Sokaras, D., Steiner, J.D., Weng, T.-C., Nordlund, D., Doeff, M.M., et al. (2018). Oxygen release induced chemomechanical breakdown of layered cathode materials. Nano Lett. *18*, 3241–3249.

121. Jacquet, Q., Iadecola, A., Saubanère, M., Li, H., Berg, E.J., Rousse, G., Cabana, J., Doublet, M.-L., and Tarascon, J.-M. (2019). Charge transfer band gap as an indicator of hysteresis in Li-disordered rock salt cathodes for Li-ion batteries. J. Am. Chem. Soc. *141*, 11452–11464.

122. Gallagher, K.G., Croy, J.R., Balasubramanian, M., Bettge, M., Abraham, D.P., Burrell, A.K., and Thackeray, M.M. (2013). Correlating hysteresis and voltage fade in lithium- and manganese-rich layered transition-metal oxide electrodes. Electrochem. Commun. *33*, 96–98.

123. Assat, G., Glazier, S.L., Delacourt, C., and Tarascon, J.-M. (2019). Probing the thermal effects of voltage hysteresis in anionic redox-based lithium-rich cathodes using isothermal calorimetry. Nat. Energy *4*, 647–656.

124. Kan, W.H., Chen, D., Papp, J.K., Shukla, A.K., Huq, A., Brown, C.M., McCloskey, B.D., and Chen, G. (2018). Unravelling solid-state redox chemistry in $Li_{1.3}Nb_{0.3}Mn_{0.4}O_2$ single-crystal cathode. Mater. Chem. Mater. *30*, 1655–1666.

125. Zhang, H., May, B.M., Omenya, F., Whittingham, M.S., Cabana, J., and Zhou, G. (2019). Layered oxide cathodes for Li-ion batteries: oxygen loss and vacancy evolution. Chem. Mater. *31*, 7790–7798.

126. Shin, Y., and Persson, K.A. (2016). Surface morphology and surface stability against oxygen loss of the lithium-excess Li_2MnO_3 cathode material as a function of lithium concentration. ACS Appl. Mater. Interfaces *8*, 25595–25602.

127. McCalla, E., Sougrati, M.T., Rousse, G., Berg, E.J., Abakumov, A., Recham, N., Ramesha, K., Sathiya, M., Dominko, R., Van Tendeloo, G., et al. (2015). Understanding the roles of anionic redox and oxygen release during electrochemical cycling of lithium-rich layered Li_4FeSbO_6. J. Am. Chem. Soc. *137*, 4804–4814.

128. Jacquet, Q., Iadecola, A., Saubanère, M., Lemarquis, L., Berg, E.J., Alves Dalla Corte, D., Rousse, G., Doublet, M.-L., and Tarascon, J.-M. (2018). Competition between metal dissolution and gas release in Li-rich $Li_3Ru_yIr_{1-y}O_4$ model compounds showing anionic redox. Chem. Mater. *30*, 7682–7690.

129. Sun, C., Liao, X., Xia, F., Zhao, Y., Zhang, L., Mu, S., Shi, S., Li, Y., Peng, H., Van Tendeloo, G., et al. (2020). High-voltage cycling induced thermal vulnerability in $LiCoO_2$ cathode: cation loss and oxygen release driven by oxygen vacancy migration. ACS Nano *14*, 6181–6190.

130. Nakamura, T., Gao, H., Ohta, K., Kimura, Y., Tamenori, Y., Nitta, K., Ina, T., Oishi, M., and Amezawa, K. (2019). Defect chemical studies on oxygen release from the Li-rich cathode material $Li_{1.2}Mn_{0.6}Ni_{0.2}O_{2-\delta}$. J. Mater. Chem. A *7*, 5009–5019.

131. Hamaguchi, M., Momida, H., and Oguchi, T. (2020). Significant role of oxygen redox reaction with O_2-release in Li-excess cation-disordered rock-salt cathodes $Li_{2+2x}Mn_{1-x}Ti_{1-x}O_4$: first-principles calculations. Electrochim. Acta *330*, 135286.

132. Marusczyk, A., Albina, J.-M., Hammerschmidt, T., Drautz, R., Eckl, T., and Henkelman, G. (2017). Oxygen activity and peroxide formation as charge compensation mechanisms in Li_2MnO_3. J. Mater. Chem. A *5*, 15183–15190.

133. Sharifi-Asl, S., Lu, J., Amine, K., and Shahbazian-Yassar, R. (2019). Oxygen release degradation in Li-ion battery cathode materials: mechanisms and mitigating approaches. Adv. Energy Mater. *9*, 1900551.

134. Yan, P., Zheng, J., Tang, Z.K., Devaraj, A., Chen, G., Amine, K., Zhang, J.-G., Liu, L.-M., and Wang, C. (2019). Injection of oxygen vacancies in the bulk lattice of layered cathodes. Nat. Nanotechnol. *14*, 602–608.

135. Lee, E., and Persson, K.A. (2014). Structural and chemical evolution of the layered Li-excess Li_xMnO_3 as a function of Li content from first-principles calculations. Adv. Energy Mater. *4*, 1400498.

136. Tian, C., Nordlund, D., Xin, H.L., Xu, Y., Liu, Y., Sokaras, D., Lin, F., and Doeff, M.M. (2018). Depth-dependent redox behavior of $LiNi_{0.6}Mn_{0.2}Co_{0.2}O_2$. J. Electrochem. Soc. *165*, A696–A704.

137. Tian, C., Xu, Y., Kan, W.H., Sokaras, D., Nordlund, D., Shen, H., Chen, K., Liu, Y., and Doeff, M. (2020). Distinct surface and bulk thermal behaviors of $LiNi_{0.6}Mn_{0.2}Co_{0.2}O_2$ cathode materials as a function of state of charge. ACS Appl. Mater. Interfaces *12*, 11643–11656.

138. Wang, H., Rus, E., Sakuraba, T., Kikuchi, J., Kiya, Y., and Abruna, H.D. (2014). CO_2 and O_2 evolution at high voltage cathode materials of Li-ion batteries: a differential electrochemical mass spectrometry study. Anal. Chem. *86*, 6197–6201.

139. Dahn, J.R., Fuller, E.W., Obrovac, M., and von Sacken, U. (1994). Thermal stability of Li_xCoO_2, Li_xNiO_2 and λ-MnO_2 and consequences for the safety of Li-ion cells. Solid State Ionics *69*, 265–270.

140. Jiang, J., and Dahn, J.R. (2005). Electrochemical and thermal studies of Li $[Ni_xLi_{(1/3-2x/3)}Mn_{(2/3-x/3)}]O_2$ (x = 1/12, 1/4, 5/12, and 1/2). Electrochim. Acta *50*, 4778–4783.

141. Steiner, J., Mu, L., Walsh, J., Rahman, M.M., Zydlewski, B., Michel, M., Xin, H.L., Nordlund, D., and Lin, F. (2018). Accelerated evolution of surface chemistry determined by temperature and cycling history in nickel-rich layered cathode materials. ACS Appl. Mater. Interfaces *10*, 23842–23850.

142. Liu, X., Yang, W., and Liu, Z. (2014). Recent progress on synchrotron-based in-situ soft X-ray spectroscopy for energy materials. Adv. Mater. *26*, 7710–7729.

143. Wu, J., Li, Q., Sallis, S., Zhuo, Z., Gent, W.E., Chueh, W.C., Yan, S., Chuang, Y., and Yang, W. (2019). Fingerprint oxygen redox reactions in batteries through high-efficiency mapping of resonant inelastic X-ray scattering. Condens. Matter *4*, 5.

144. Ma, L.A., Massel, F., Naylor, A.J., Duda, L.-C., and Younesi, R. (2019). Understanding charge compensation mechanisms in $Na_{0.56}Mg_{0.04}Ni_{0.19}Mn_{0.70}O_2$. Commun. Chem. *2*, https://doi.org/10.1038/s42004-019-0227-z.

145. Zhuo, Z., Olalde-Velasco, P., Chin, T., Battaglia, V., Harris, S.J., Pan, F., and Yang, W. (2017). Effect of excess lithium in $LiMn_2O_4$ and $Li_{1.15}Mn_{1.85}O_4$ electrodes revealed by quantitative analysis of soft X-ray absorption spectroscopy. Appl. Phys. Lett. *110*, 093902.

146. Shen, S., Hong, Y., Zhu, F., Cao, Z., Li, Y., Ke, F., Fan, J., Zhou, L., Wu, L., Dai, P., et al. (2018). Tuning electrochemical properties of Li-rich layered oxide cathodes by adjusting Co/Ni ratios and mechanism investigation using in situ X-ray diffraction and online continuous flow differential electrochemical mass

spectrometry. ACS Appl. Mater. Interfaces *10*, 12666–12677.

147. Castel, E., Berg, E.J., El Kazzi, M., Novák, P., and Villevieille, C. (2014). Differential electrochemical mass spectrometry study of the interface of $xLi_2MnO_{3(1-x)}LiMO_2$ (M = Ni, Co, and Mn) material as a positive electrode in Li-ion batteries. Chem. Mater. *26*, 5051–5057.

148. Yan, J., Liu, X., and Li, B. (2014). Recent progress in Li-rich layered oxides as cathode materials for Li-ion batteries. RSC Adv. *4*, 63268–63284.

149. Wandt, J., Freiberg, A.T.S., Ogrodnik, A., and Gasteiger, H.A. (2018). Singlet oxygen evolution from layered transition metal oxide cathode materials and its implications for lithium-ion batteries. Mater. Today *21*, 825–833.

150. Boulineau, A., Simonin, L., Colin, J.-F., Canévet, E., Daniel, L., and Patoux, S. (2012). Evolutions of $Li_{1.2}Mn_{0.61}Ni_{0.18}Mg_{0.01}O_2$ during the initial charge/discharge cycle studied by advanced electron microscopy. Chem. Mater. *24*, 3558–3566.

151. Boulineau, A., Simonin, L., Colin, J.-F., Bourbon, C., and Patoux, S. (2013). First evidence of manganese-nickel segregation and densification upon cycling in Li-rich layered oxides for lithium batteries. Nano Lett. *13*, 3857–3863.

152. Gu, M., Belharouak, I., Zheng, J., Wu, H., Xiao, J., Genc, A., Amine, K., Thevuthasan, S., Baer, D.R., Zhang, J.-G., et al. (2013). Formation of the spinel phase in the layered composite cathode used in Li-ion batteries. ACS Nano *7*, 760–767.

153. Zheng, J., Xu, P., Gu, M., Xiao, J., Browning, N.D., Yan, P., Wang, C., and Zhang, J.-G. (2015). Structural and chemical evolution of Li- and Mn-rich layered cathode material. Chem. Mater. *27*, 1381–1390.

154. Xu, B., Fell, C.R., Chi, M., and Meng, Y.S. (2011). Identifying surface structural changes in layered Li-excess nickel manganese oxides in high voltage lithium ion batteries: a joint experimental and theoretical study. Energy Environ. Sci. *4*, 2223–2233.

155. Jiang, Z., Li, J., Yang, Y., Mu, L., Wei, C., Yu, X., Pianetta, P., Zhao, K., Cloetens, P., Lin, F., et al. (2020). Machine-learning-revealed statistics of the particle-carbon/binder detachment in lithium-ion battery cathodes. Nat. Commun. *11*, 2310.

156. Xu, Z., Rahman, M.M., Mu, L., Liu, Y., and Lin, F. (2018). Chemomechanical behaviors of layered cathode materials in alkali metal ion batteries. J. Mater. Chem. A *6*, 21859–21884.

157. Li, Q., Li, G., Fu, C., Luo, D., Fan, J., and Li, L. (2014). K^+-doped $Li_{1.2}Mn_{0.54}Co_{0.13}Ni_{0.13}O_2$: a novel cathode material with an enhanced cycling stability for lithium-ion batteries. ACS Appl. Mater. Interfaces *6*, 10330–10341.

158. Eum, D., Kim, B., Kim, S.J., Park, H., Wu, J., Cho, S.-P., Yoon, G., Lee, M.H., Jung, S.-K., Yang, W., et al. (2020). Voltage decay and redox asymmetry mitigation by reversible cation migration in lithium-rich layered oxide electrodes. Nat. Mater. *19*, 419–427.

159. Ku, K., Hong, J., Kim, H., Park, H., Seong, W.M., Jung, S.-K., Yoon, G., Park, K.-Y., Kim, H., and Kang, K. (2018). Suppression of voltage decay through manganese deactivation and nickel redox buffering in high-energy layered lithium-rich electrodes. Adv. Energy Mater. *8*, 1800606.

160. Shi, J.L., Zhang, J.-N., He, M., Zhang, X.-D., Yin, Y.-X., Li, H., Guo, Y.-G., Gu, L., and Wan, L.-J. (2016). Mitigating voltage decay of Li-rich cathode material via increasing Ni content for lithium-ion batteries. ACS Appl. Mater. Interfaces *8*, 20138–20146.

161. Zhu, Z., Yu, D., Yang, Y., Su, C., Huang, Y., Dong, Y., Waluyo, I., Wang, B., Hunt, A., Yao, X., et al. (2019). Gradient Li-rich oxide cathode particles immunized against oxygen release by a molten salt treatment. Nat. Energy *4*, 1049–1058.

162. Zhang, S., Gu, H., Pan, H., Yang, S., Du, W., Li, X., Gao, M., Liu, Y., Zhu, M., Ouyang, L., et al. (2017). A novel strategy to suppress capacity and voltage fading of Li- and Mn-rich layered oxide cathode material for lithium-ion batteries. Adv. Energy Mater. *7*, 1601066.

163. Chen, D., Zheng, F., Li, L., Chen, M., Zhong, X., Li, W., and Lu, L. (2017). Effect of Li_3PO_4 coating of layered lithium-rich oxide on electrochemical performance. J. Power Sources *341*, 147–155.

164. Song, B., Li, W., Oh, S.-M., and Manthiram, A. (2017). Long-life nickel-rich layered oxide cathodes with a uniform Li_2ZrO_3 surface coating for lithium-ion batteries. ACS Appl. Mater. Interfaces *9*, 9718–9725.

165. Nisar, U., Petla, R., Jassim Al-Hail, S.A., Quddus, A.A., Monawwar, H., Shakoor, A., Essehli, R., and Amin, R. (2020). Impact of surface coating on electrochemical and thermal behaviors of a Li-rich $Li_{1.2}Ni_{0.16}Mn_{0.56}Co_{0.08}O_2$ cathode. RSC Adv. *10*, 15274–15281.

166. Nisar, U., Amin, R., Essehli, R., Shakoor, R.A., Kahraman, R., Kim, D.K., Khaleel, M.A., and Belharouak, I. (2018). Extreme fast charging characteristics of zirconia modified $LiNi_{0.5}Mn_{1.5}O_4$ cathode for lithium ion batteries. J. Power Sources *396*, 774–781.

167. Li, X., Zhang, K., Mitlin, D., Yang, Z., Wang, M., Tang, Y., Jiang, F., Du, Y., and Zheng, J. (2018). Fundamental insight into Zr modification of Li- and Mn-rich cathodes: combined transmission electron microscopy and electrochemical impedance spectroscopy study. Chem. Mater. *30*, 2566–2573.

168. Lee, K.-S., Myung, S.-T., Bang, H., Amine, K., Kim, D.-W., and Sun, Y.-K. (2009). Effect of protecting metal oxide (Co_3O_4) layer on electrochemical properties of spinel $Li_{1.1}Mn_{1.9}O_4$ as a cathode material for lithium battery applications. J. Power Sources *189*, 494–498.

169. Gao, K., Zhao, S.-X., Guo, S.-T., and Nan, C.-W. (2016). Improving rate capacity and cycling performance of lithium-rich high-Mn $Li_{1.8}[Mn_{0.7}Co_{0.15}Ni_{0.15}]O_{2.675}$ cathode materials by Li_2SiO_3 coating. Electrochim. Acta *206*, 1–9.

170. Li, B., Wang, J., Cao, Z., Zhang, P., and Zhao, J. (2016). The role of SnO_2 surface coating in the electrochemical performance of $Li_{1.2}Mn_{0.54}Co_{0.13}Ni_{0.13}O_2$ cathode materials. J. Power Sources *325*, 84–90.

171. Kobayashi, G., Irii, Y., Matsumoto, F., Ito, A., Ohsawa, Y., Yamamoto, S., Cui, Y., Son, J.-Y., and Sato, Y. (2016). Improving cycling performance of Li-rich layered cathode materials through combination of Al_2O_3-based surface modification and stepwise precycling. J. Power Sources *303*, 250–256.

172. Zhang, X., Belharouak, I., Li, L., Lei, Y., Elam, J.W., Nie, A., Chen, X., Yassar, R.S., and Axelbaum, R.L. (2013). Structural and electrochemical study of Al_2O_3 and TiO_2 coated $Li_{1.2}Ni_{0.13}Mn_{0.54}Co_{0.13}O_2$ cathode material using ALD. Adv. Energy Mater. *3*, 1299–1307.

173. Liao, J.-Y., and Manthiram, A. (2015). Surface-modified concentration-gradient Ni-rich layered oxide cathodes for high-energy lithium-ion batteries. J. Power Sources *282*, 429–436.

174. Sun, Y.-K., Lee, M.-J., Yoon, C.S., Hassoun, J., Amine, K., and Scrosati, B. (2012). The role of AlF_3 coatings in improving electrochemical cycling of Li-enriched nickel-manganese oxide electrodes for Li-ion batteries. Adv. Mater. *24*, 1192–1196.

175. Zhang, W., Sun, Y., Deng, H., Ma, J., Zeng, Y., Zhu, Z., Lv, Z., Xia, H., Ge, X., Cao, S., et al. (2020). Dielectric polarization in inverse spinel-structured Mg_2TiO_4 coating to suppress oxygen evolution of Li-rich cathode materials. Adv. Mater. *32*, e2000496.

176. Hu, S., Li, Y., Chen, Y., Peng, J., Zhou, T., Pang, W.K., Didier, C., Peterson, V.K., Wang, H., Li, Q., et al. (2019). Insight of a phase compatible surface coating for long-durable Li-rich layered oxide cathode. Adv. Energy Mater. *9*, 1901795.

177. Zhang, K., Kim, D., Hu, Z., Park, M., Noh, G., Yang, Y., Zhang, J., Lau, V.W., Chou, S.-L., Cho, M., et al. (2019). Manganese based layered oxides with modulated electronic and thermodynamic properties for sodium ion batteries. Nat. Commun. *10*, 5203.

178. Xie, Q., Li, W., and Manthiram, A. (2019). A Mg-doped high-nickel layered oxide cathode enabling safer, high-energy-density Li-ion batteries. Chem. Mater. *31*, 938–946.

179. Li, C., Zhao, C., Hu, B., Tong, W., Shen, M., and Hu, B. (2020). Unraveling the critical role of Ti substitution in P2-$Na_xLi_yMn_{1-y}O_2$ cathodes for highly reversible oxygen redox chemistry. Chem. Mater. *32*, 1054–1063.

180. Ming, L., Zhang, B., Cao, Y., Zhang, J.-F., Wang, C.-H., Wang, X.-W., and Li, H. (2018). Effect of Nb and F co-doping on $Li_{1.2}Mn_{0.54}Ni_{0.13}Co_{0.13}O_2$ cathode material for high-performance lithium-ion batteries. Front. Chem. *6*, 76.

181. Pang, W.K., Lin, H.-F., Peterson, V.K., Lu, C.-Z., Liu, C.-E., Liao, S.-C., and Chen, J.-M. (2017). Effects of fluorine and chromium doping on the performance of lithium-rich $Li_{1+x}MO_2$ (M = Ni, Mn, Co) positive electrodes. Chem. Mater. *29*, 10299–10311.

182. Park, S.H., and Sun, Y.-K. (2003). Synthesis and electrochemical properties of layered Li $[Li_{0.15}Ni_{(0.275-x/2)}Al_xMn_{(0.575-x/2)}]O_2$ materials

prepared by sol-gel method. J. Power Sources *119-121*, 161–165.

183. Sha, O., Tang, Z., Wang, S., Yuan, W., Qiao, Z., Xu, Q., and Ma, L. (2012). The multi-substituted $LiNi_{0.475}Al_{0.01}Cr_{0.04}Mn_{1.475}O_{3.95}F_{0.05}$ cathode material with excellent rate capability and cycle life. Electrochim. Acta *77*, 250–255.

184. Tabuchi, M., Nabeshima, Y., Takeuchi, T., Kageyama, H., Tatsumi, K., Akimoto, J., Shibuya, H., and Imaizumi, J. (2011). Synthesis and electrochemical characterization of Fe and Ni substituted Li_2MnO_3—an effective means to use Fe for constructing "Co-free" Li_2MnO_3 based positive electrode material. J. Power Sources *196*, 3611–3622.

185. Kim, Y. (2019). Effects and distribution of Zr introduced in Ni-based cathode material for Li-ion batteries. Phys. Chem. Chem. Phys. *21*, 12505–12517.

186. Yu, Z., Ning, F., Li, B., Sun, Z., Chu, W., and Xia, D. (2019). Mitigating voltage decay of Li-rich layered oxide by incorporation of 5d metal rhenium. J. Phys. Chem. C *123*, 18870–18876.

187. Richards, W.D., Dacek, S.T., Kitchaev, D.A., and Ceder, G. (2018). Fluorination of lithium-excess transition metal oxide cathode materials. Adv. Energy Mater. *8*, 1701533.

188. Steiner, J.D., Cheng, H., Walsh, J., Zhang, Y., Zydlewski, B., Mu, L., Xu, Z., Rahman, M.M., Sun, H., Michel, F.M., et al. (2019). Targeted surface doping with reversible local environment improves oxygen stability at the electrochemical interfaces of nickel-rich cathode materials. ACS Appl. Mater. Interfaces *11*, 37885–37891.

189. Das, S., Wang, B., Cao, Y., Rae Cho, M., Jae Shin, Y., Yang, S.M., Wang, L., Kim, M., Kalinin, S.V., Chen, L.-Q., et al. (2017). Controlled manipulation of oxygen vacancies using nanoscale flexoelectricity. Nat. Commun. *8*, 615.

190. Wu, J., Zhang, X., Zheng, S., Liu, H., Wu, J., Fu, R., Li, Y., Xiang, Y., Liu, R., Zuo, W., et al. (2020). Tuning oxygen redox reaction through the inductive effect with proton insertion in Li-rich oxides. ACS Appl. Mater. Interfaces *12*, 7277–7284.

191. Huang, J., Liu, H., Hu, T., Meng, Y.S., and Luo, J. (2018). Enhancing the electrochemical performance of Li-rich layered oxide $Li_{1.13}Ni_{0.3}Mn_{0.57}O_2$ via WO_3 doping and accompanying spontaneous surface phase formation. J. Power Sources *375*, 21–28.

192. Zhang, J.-N., Li, Q., Ouyang, C., Yu, X., Ge, M., Huang, X., Hu, E., Ma, C., Li, S., Xiao, R., et al. (2019). Trace doping of multiple elements enables stable battery cycling of $LiCoO_2$ at 4.6 V. Nat. Energy *4*, 594–603.

193. Yang, Z., Mu, L., Hou, D., Rahman, M.M., Xu, Z., Liu, J., Nordlund, D., Sun, C., Xiao, X., and Lin, F. (2020). Probing dopant redistribution, phase propagation, and local chemical changes in the synthesis of layered oxide battery cathodes. Adv. Energy Mater. https://doi.org/10.1002/aenm.202002719.

194. Van der Ven, A., Aydinol, M.K., Ceder, G., Kresse, G., and Hafner, J. (1998). First-principles investigation of phase stability. Phys. Rev. B Condens. Matter Mater. Phys. *58*, 2975–2987.

195. Rana, J., Papp, J.K., Lebens-Higgins, Z., Zuba, M., Kaufman, L.A., Goel, A., Schmuch, R., Winter, M., Whittingham, M.S., Yang, W., et al. (2020). Quantifying the capacity contributions during activation of Li_2MnO_3. ACS Energy Lett. *5*, 634–641.

196. Xu, J., Sun, M., Qiao, R., Renfrew, S.E., Ma, L., Wu, T., Hwang, S., Nordlund, D., Su, D., Amine, K., et al. (2018). Elucidating anionic oxygen activity in lithium-rich layered oxides. Nat. Commun. *9*, 947.

197. Van Bommel, A., and Dahn, J.R. (2010). Kinetics study of the high potential range of lithium-rich transition-metal oxides for lithium-ion batteries by electrochemical methods. Electrochem. Solid State Lett. *13*, A62.

198. Kim, H.J., Konarov, A., Jo, J.H., Choi, J.U., Ihm, K., Lee, H., Kim, J., and Myung, S. (2019). Controlled oxygen redox for excellent power capability in layered sodium-based compounds. Adv. Energy Mater. *9*, 1901181.

199. Xu, H., Guo, S., and Zhou, H. (2019). Review on anionic redox in sodium-ion batteries. J. Mater. Chem. A *7*, 23662–23678.